SCHOOL OF ELECTRICAL ENGINEERING
AND TELECOMMUNICATIONS

Beamforming Design for Secure IRS-assisted Networks

by

Mao Li

Student ID: z5346632

Thesis submitted as a requirement for the degree

Master of Engineering (Telecommunications)

Submitted: December 3, 2023
Supervisor: Derrick Wing Kwan Ng

Abstract

This thesis contributes to delivering a specific outline for one type of beamforming design with Intelligent Reflecting Surface (IRS) technology in future 6G secure networks. It is also dedicated to developing one flexible beamforming design model with the following specific problem formulation and algorithm design for improving the sum secrecy rate of one certain IRS-assisted network by applying an Unmanned Aerial Vehicle (UAV) and sacrificing a range of legitimate users with a low Signal-to-Interference-Plus-Noise (SINR) Ratio. The whole design can be categorised as a resource allocation issue, thus, some convex optimisation methods such as alternating optimisation and oblique manifold optimization are used in the algorithm design process and the relevant simulation results are analysed and explained in the end. The purposes of combining UAV and IRS and applying the user-sacrificing technique are to increase flexibility to a large extent by introducing a new factor height to the network and to improve the security of this system under certain resource constraints.

Abbreviations

1G First-Generation of Wireless Communication Technology

2G Second-Generation of Wireless Communication Technology

3G Third-Generation of Wireless Communication Technology

4G Forth-Generation of Wireless Communication Technology

5G Fifth-Generation of Wireless Communication Technology

6G Sixth-Generation of Wireless Communications Technology

AI Artificial Intelligence

AO Alternating Optimization

BS Base Station

CDMA Code Division Multiple Access

CSI Channel State Information

DAS Distributed Antenna Systems

DoF Degrees-of-Freedom

ED Eavesdropper

EH Energy Harvesting

FD Full-duplex

FDMA Frequency Division Multiple Access

GSM Global System for Mobile Communication

HD Half-duplex

HSPA High Speed Packet Access

IoT Internet-of-Things

IP Internet Protocol

IRS Intelligent Reflecting Surface

LU Legitimate User

LOS Line-of-Sight

MIMO Multiple Input Multiple Output

MISO Multiple Input Single Output

ML Machine Learning

NFV Network Function Virtualization

NOMA Non-orthogonal Multiple Access

NLOS Non-Line-of-Sight

OFDM Orthogonal Frequency Division Multiplexing

OMO Oblique Manifold Optimization

PLS Physical Layer Security

PIN Positive Intrinsic Negative

QoS Quality of Service

RF Radio Frequency

SCA Successive Convex Approximation

SDN Software-Defined Networking

SDR Semidefinite Relaxation

SMS Short Message Service

STAR-RIS Simultaneously Transmitting and Reflecting Reconfigurable Intelligent Surface

SU Selected User

SNR Signal-to-Noise Ratio

SINR Signal-to-Interference-Plus-Noise Ratio

SWIPT Simultaneous Wireless Information and Power Transfer

TDMA Time Division Multiple Access

UAV Unmanned Aerial Vehicle

URLLC Ultra-Reliable Low Latency Communication

WCDMA Wideband Code Division Multiple Access

WPT Wireless Power Transfer

Notations

$\mathcal{L}$ Total number of legitimate users

$\mathcal{M}$ Total number of eavesdroppers

$\mathcal{D}$ Total number of selected users

γ_{min} The minimum required SINR

$\mathbf{H}$ BS-to-IRS Link

$\mathbf{h}_{\boldsymbol{d}}^{H}$ BS-to-LU Direct Link

$\mathbf{h}_{\boldsymbol{r}}^{H}$ IRS-to-LU link

$\mathbf{g}_{\boldsymbol{d}}^{H}$ BS-to-ED Direct Link

$\mathbf{g}_{\boldsymbol{r}}^{H}$ IRS-to-ED link

$\mathbf{w}_i$ Beamforming vector

$\mathbf{a}$ Artificial noise vector

s_i Information signals

Φ Phase matrix of IRS

z Altitude of the UAV

$\mathcal{Z}_{max}$ The maximum height of the UAV

$\mathcal{Z}_{min}$ The minimum height of the UAV

$\beta(z)$ Attenuation function of z

Contents

Chapter 1

Introduction

Wireless communication [1] has been influencing the daily life of everyone gradually, the concept of wireless communication can be tracked to the second half of the nineteenth century since James Clerk Maxwell formed his famous theory of electromagnetism [2]. Maxwell's equations reveal the underlying association between electric and magnetic fields which further led to the discovery of electromagnetic waves [3] by Heinrich Hertz. The electromagnetic wave is exactly the medium to convey information from one side to another side which people officially define as the 'radio wave' or 'signal'. It is widely acknowledged that all the traditional wireless communication techniques are rooted in Maxwell's electromagnetic theory and Hertz's experimental work. Many mathematicians, physicists and engineers such as Harold Stephen Black, Guglielmo Marconi, and Claude Shannon are involved in the revolution of wireless communication. At the same time, other pioneers in physics and mathematics domain such as Johann Carl Friedrich Gauss, Nikola Tesla, Joseph Fourier, and Joseph-Louis Lagrange had laid solid theoretical stepping stones for others to develop wireless communication.

The evolution of wireless communication in recent years can be categorised by the term 'generation' and each generation normally lasts ten years, which means that a neoteric era of wireless communication technology will emerge every ten years [4]. A number of basic concepts and primitive technologies were found out and invented within the first three generations which also acted as supporting backbones for the further generations. The first generation (1G) [5] started in the late 1970s with its epochmaking analog cellular communicating technology [5] and Frequency Division Multiple Access (FDMA) technology [6]. 1G is Followed by the second generation (2G) [7] with new features such as Global System for Mobile Communications (GSM) [7], Time Division Multiple Access (TDMA) [8] and Code Division Mul-

tiple Access (CDMA) [9] in the 1990s, frequency bands suddenly became essential resources. The common services for users are simply voice communication and Short Message Service (SMS) [10]. For the third generation of wireless communication (3G) [11], the most significant improvements are the birth of Wideband Code Division Multiple Access (WCDMA) technique [12] and High Speed Packet Access (HSPA) techniques [13] which largely increases the speed of data transmission between the users and the Internet and the capacity of the communication channel. From 1G to 3G, wireless communications became more and more normal and accessible for everyone, related radio services and data services such as real-time voice calls, SMS and data roaming changed the way of communication forever. It was also during this era that the Internet announced its epic victory in pumping into people's daily lives for the first time because it officially became an essential part of wireless communications. Meanwhile, The first three generations really had a huge impact on telecommunications by establishing plenty of novel thoughts and original theories that can always potentially throw questions out for people in the future to explore and research.

The most significant improvement for the fourth generation of wireless communication technology (4G) [14] is the extremely high data rate compared with the last three generations, which can be credited to the universally acclaimed Orthogonal Frequency Division Multiplexing (OFDM) [15]. OFDM technology has largely extended the signal coverage by overcoming the frequency selective fading and made a huge progress on mitigating of signal interference. It was also in the 4G era that the Unmanned Aerial Vehicle (UAV) [16] first served telecommunication as an innovative technology and UAV contributed to 4G in many ways due to its multiple useful and adaptable functions. For example, its unique flexible mobility feature also allows UAVs to enlarge the signal coverage of receivers and the embedded technology enables UAVs to constantly update different functions which further increases the adaptability of combining other technologies. In other words, these characteristics do change the way the transmitter and the receiver communicate. Meanwhile, Multiple Input Single Output (MISO) [17] and Multiple Input Multiple Output (MIMO) [18] technologies. Many extraordinary outcomes such as high data rate and long-distance signal transmission can be achieved by applying the MISO and MIMO technology.

At the moment, people are overwhelmed by the enormous benefits brought by the fifth generation of wireless communication technology (5G) [19], those benefits can be simply listed as higher upload and download data rates which is also the speed of transceiving data, better en-

ergy efficiency, lower latency between the transmitter side and receiver side, and greater capacity to support more devices within the communication cellular region. The reason behind that development is the revolution of networking industries, new techniques such as Network Function Virtualization (NFV) [20] and Software-Defined Networking (SDN) [21] totally changed the quality of network services. At the same time, other techniques like Ultra-Reliable Low Latency Communication (URLLC) [22] and beamforming technique [23] also play an extremely essential role within the 5G.

The sixth generation of wireless communication technology (6G) [24] is supposed to be complemented for the market to use around the 2030s. As a marvellous brunch of 6G technology, Intelligent Reflecting Surface (IRS) [25] owns one important place on the stage and all the contents introduced before have paved the way for IRS technology to some extent, Figure 1.1 shows a clear flowchart about different generations which finally leads to IRS during the development of wireless communication. There are a lot of applications that contain IRS-assisted technology, such as energy efficiency design [26], beamforming design [27], signal interference management [28], combination with Internet-of-Things (IoT) [29], contribution to MISO and MIMO systems. For instance, the IRS has already been used in practice successfully in the 19th Asian Games in Hangzhou. In addition, These IRS-assisted applications are absolutely linked with resource allocation [30] which is generally an optimisation algorithm design problem at the same time. The aim of resource allocation optimisation problems can be achieved by judging, evaluating and balancing multiple idiographic trade-offs under certain limitations. Technically, those optimisation problems are normally complicated non-convex problems [31] and hard to analyse and solve. Particularly, the rise of Artificial Intelligence (AI) [32] may become a good sign for solving the above optimisation problems. Furthermore, more and more people become interested in the concept of Green and Sustainable Communication [33], which can also be a highlight of 6G.

This thesis aims to complete one comprehensive beamforming design for secure IRS-assisted networks for a specific scenario in practice. The prerequisite background knowledge is expounded in Chapter 2. Chapter 3 is placed for the relevant literature reviews in the IRS and UAV domains. A system model is well-designed with the following problem formulation shown in Chapter 4, this part explains the outline and every necessary detail of the UAV-assisted IRS system which will be taken into consideration in the following chapters. Chapter 5 contains meticulous analyses of the optimisation problem. Chapter 6 displays the final simulation

results and can be used to evaluate the performance of the designed algorithm. Subsequently, a summary and further research directions such as some physical constraints to this system model and future development of the UAV and IRS are stated in Chapter 7.

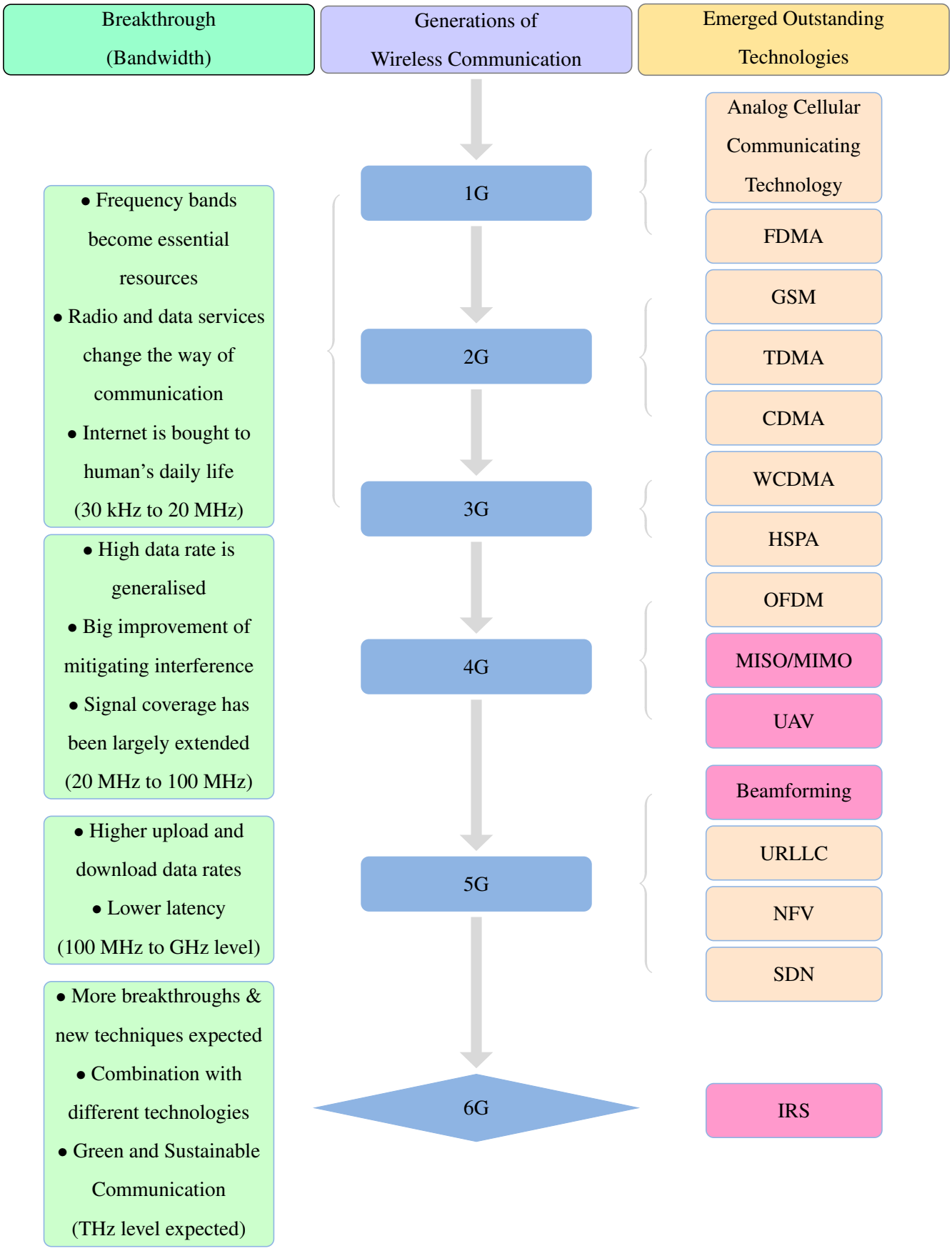

Figure 1.1: Flowchart of the development of IRS-related wireless communication

Chapter 2

Background

2.1 Beamforming concept

The fundamental principle behind IRS is beamforming, a very helpful and popular technique for directing signals in one preferred direction. Those signals are normally generated by multiple antennas, which are usually equipped on both sides of the transmitter and receiver. In order to throw out the multiple antenna scenario with a more accepting sense, a single antenna case is introduced at first. Figure 2.1 illustrates the signal range generated by one single antenna, which can be approximated to a semicircular sector. This sector is named 'signal lobe' indicating the coverage of the signal. In this case, the signal has no 'preferred' direction to arrive within this half-circular range. Furthermore, the signal lobe becomes a hemispherical shape in the three-dimensional space, which significantly increases the difficulty of controlling the signal. And every signal from the antenna can be noted mathematically by a sinusoidal function $sin(t)$ or similarly '$\alpha e^{j\theta}$', where α and θ denote the amplitude and phase of the signal. Meanwhile, as long as the distance and medium between the signal and the antenna are fixed, the amplitude and phase of each signal are the same. Because both the energy loss and the delay 'τ' to the signal are related to the distance. This theorem is extremely vital because it reveals the relationship between the distance away from the antenna and the information of the signal. Thus, the only method to enlarge the signal lobe is increasing the transmission power since the path loss factor is fixed in one practical environment, which is really inefficient in reality. In addition, the one single antenna transmission scenario is the most straightforward way of sending the signal, but it is also the most essential foundation that leads to other techniques of wireless communication.

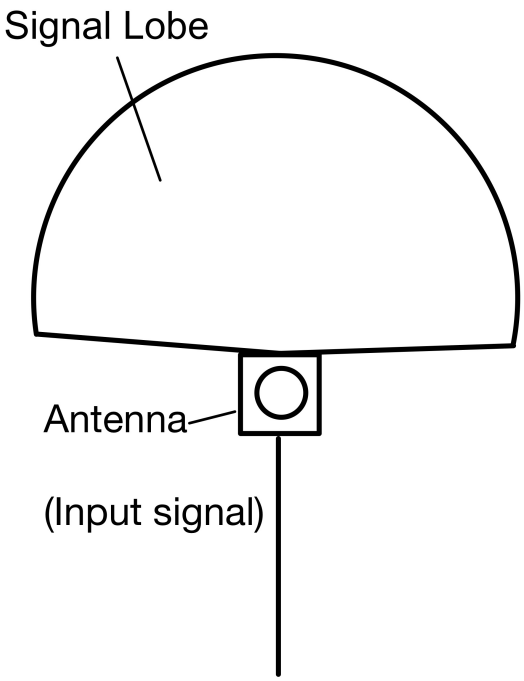

Figure 2.1: The signal lobe of one antenna

However, there are no base stations (BS) that only assemble one antenna nowadays and multiple antenna scenario is widely accepted in modern wireless communication networks. This is due to the fact that multiple antenna can satisfy huge demands of the customers by transmitting multiple different signals at one time, which leads to the multiple antenna technologies [34] later. More importantly, the matters are not only connected to distance anymore, other issues such as signal interference, antennas' position and the mobility of the users also need to be taken into consideration seriously by telecommunication professionals.

It is known that signals with the same phase add up together leading to a stronger combination of signal amplitude. On the contrary, the superposition of signals with completely opposite phases will greatly reduce the strength of the synthesized signal. Thus, it is possible to change the amplitude of the joint signal by manipulating the phase θ without changing the emission energy at the transmission side. On the other hand, the decay of signal energy is inversely proportional to the signal shuttle distance. Therefore, the amplitude of the combined signal can be maximised so long as the signals at this specific location with a fixed distance are in phase with each other and the direction from the antennas to this location is actually the direction of

the signal. besides, the Antenna number also plays an inescapable role in affecting the signal strength and signal phase. Figure 2.2 shows the connections between those discussed factors.

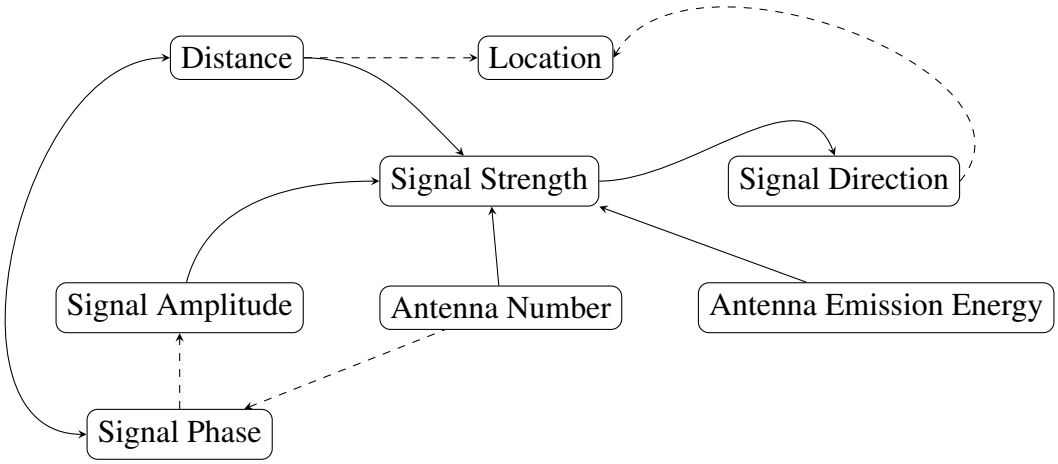

Figure 2.2: Links between the signal's characteristics and antenna

Beamforming can be briefly summarised as a technique to adjust the direction of signals by properly managing the interference between signals, which is exactly the summation of every signal's phase at one point at one time. It can be exhibited by an example of four antennas with phase shifters, shown in Figure 2.3. Theoretically, the signals of the same synchronously emitted by four horizontally arranged antennas will mainly be transmitted along the central axis. However, it is not difficult to see from Figure 2.3 that after adding the phase shift to each antenna, the main lobe is inclined at a certain angle with the central axis of the antenna panel which fully illustrates the importance of signal phase adjustment in beamforming. The direction of the main lobe can be determined by those phase shifters.

By applying the beamforming technique, the signal cover range can be extended, the interference between different signals can be deduced, and the energy consumption for the BS can be decreased. In general, the capacity of the wireless network can be increased efficiently. Furthermore, the security of legitimate users can be improved by limiting signal leakage and making it harder for eavesdroppers to intercept signals. As mentioned before, the signal travels in a three-dimensional way, thus, another highlight of beamforming is that it can support spatial multiplexing, allowing multiple data streams to be transmitted simultaneously on the same frequency leading to increasing data rates.

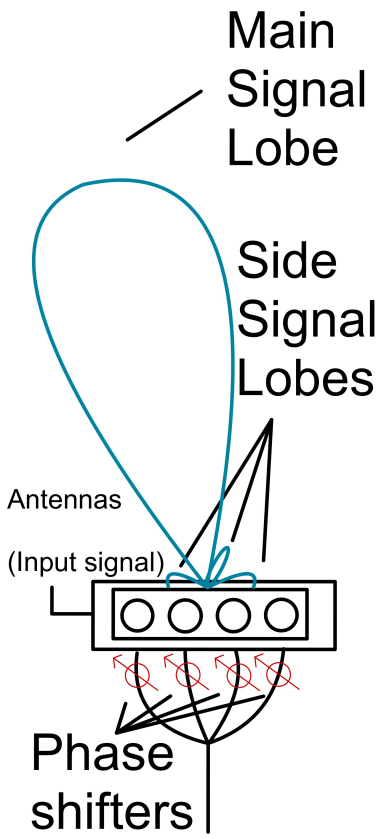

Figure 2.3: The signal lobes of four antennas

2.2 Intelligent reflecting surface

An Intelligent Reflecting Surface (IRS) is one surface formed by many tiny and passive circuit elements, which inherits most of the advantages of beamforming technique. Each element of IRS is constructed by passive circuit components such as resistors, capacitors, inductors, and even semiconductors, etc. For example, Positive Intrinsic Negative (PIN) diodes can be used in IRS element designs and each component can modify the amplitude and phase of the input signal and reflect the input signal. Those reflecting elements are similar to the phase shifters introduced before because the amplitude of the signals won't be changed normally by those passive elements. Figure 2.4 represents a basic IRS model with direct link and reflected link. The direct link is clearly one line of Line-of-Sight (LOS) link because there are no obstructions or barriers between the users and the BS. However, due to the sophisticated city structure and the uncertain variation in the environment, it's almost impossible to achieve the LOS link. Hence, Non-Line-of-Sight (NLOS) scenarios dominate the path between Bs and users and will always be considered by the urban wireless communication system.

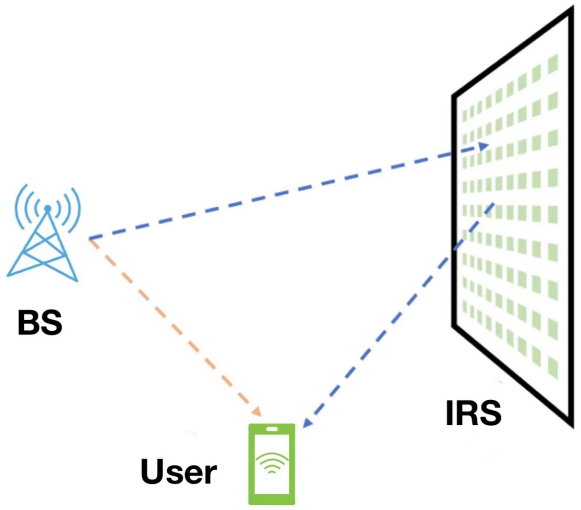

Figure 2.4: Basic IRS model

Since the principle of IRS deployment is using the IRS to 'connect' the transmitter and the receiver, in this manner a virtual LOS path can be constructed and the NLOS issue can be overcome perfectly. At the same time, it is not necessary for the IRS to be deployed on the direct path, which greatly enlarges the flexibility of the IRS.

There already exist several applications to establish the virtual LOS path, such as repeater and relay. For a repeater, it only amplifies the signal after receiving and sending it in the end. The repeater doesn't process the signal, unlike the relay which processes the received signal and then retransmits it. Moreover, relays are more intelligent and can handle advanced tasks like protocol conversion or signal translation. This is because compared with adding antennas, the overall cost for IRS passive elements is extremely low. The comparison forms for repeater, relay and IRS are listed in Figure 2.5.

Criteria / Name	Cost	Characteristics	Best deploy position	Intelligence
Repeater	high	passive	edge of the cell	low
Relay	high	active	within the cell	medium
IRS	low	passive	within the cell	high

Figure 2.5: Comparison between IRS, relay, repeater

2.3 Unmanned aerial vehicle

Unmanned Aerial Vehicle (UAV) technology stands for specific aircraft that have no pilots inside the drone and are controlled remotely by an operation control. The concept of UAV was formed a long time ago and the earliest prototype Radioplane OQ-2 [35] was invented by the U.S. military during World War II. From the blueprint of Radioplane OQ-2 shown in Figure 2.6, it's not hard to tell there is only one single bare antenna on the top of the fabric, which is similar to early remote control robots. The wireless communication is achieved between the remote control and Radioplane OQ-2 itself and this is the most fundamental UAV communication, just one UAV and one remote control.

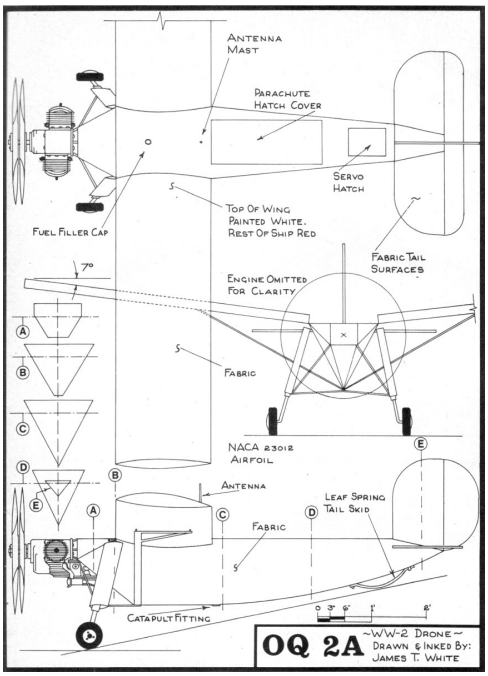

Figure 2.6: Radioplane OQ-2 blueprint

It is very hard to evaluate the performance of UAVs since the application range of UAVs is very wide. Many application scenarios exist such as remote-controlled toy planes, military detection and attack, search and rescue operations, aerial photography, disaster monitoring and traffic patrol, etc. Many of those instances are involved with information sharing and data transfer through wireless signals, which are the essence of wireless communication. Nowadays, wireless communication experts pay more attention to the research of UAV algorithms [36].

2.4 Resource allocation

As mentioned in Chapter 1, the spectrum of electromagnetic waves has become a valuable resource since people opened the gate of the wireless communication world. In the field of telecommunication, there are many resources other than the electromagnetic spectrum such as power, funds, Internet Protocol (IP) Addresses, data storage, and even satellite orbits. All of them are various kinds of resources, but they all have one thing in common, their value and amount are limited rather than inexhaustible. How to properly distribute them really becomes a realistic issue and always the first priority of any project in the beginning. Therefore, a number of scholars are delicate in researching resource allocation [37] in wireless networks. The resource allocation process often requires accurate planning, multiple monitoring, and swift and effective adjustment as conditions change. Similar to other wireless technologies, the development of the IRS and UAV technologies are inseparable from resource allocation. The most classical resource allocation examples of wireless communication are the Wireless Power Transfer (WPT) and the Simultaneous Wireless Information and Power Transfer (SWIPT) technology [38] which enables wireless devices to receive both information and electrical power simultaneously from a transmitter. One vital standard of resource allocation is Quality of Service (QoS) [39] which is to manage and prioritize the delivery of data or services to ensure a certain level of excellent performance, reliability, and quality for specific applications or users by using a set of technologies, techniques and strategies.

2.5 Physical layer security

Although wireless technology keeps providing convenience to humans in many aspects, the corresponding challenges follow closely and never stop at the same time. One of the most concerning issues is the security of communication which has been frequently discussed for many years. Security of communication can be explained as the measures to protect data and information transmitted over wireless networks from anyone except the expected legitimate receivers. Those unauthorised receivers who want to access that information and data are called 'eavesdroppers' in the telecommunication discipline. One of the most straightforward ways to improve the security of wireless communication is to enhance the protection of the transmission link between the transmitter and receiver which is also known as the wireless channel, this can be achieved by strengthening the physical layer security (PLS) [40]. Meanwhile, the

term channel state information (CSI) [41] is used to illustrate the information about the characteristics and quality of a communication channel at a given moment which can be utilised to optimise the physical layer. Parallel to resource allocation, the criterion to judge the security is called secrecy rate [42] in wireless communication. Basically, a higher secrecy rate reflects a safer network and the majority of researchers are trying to achieve their systems' secrecy rates as close as the theoretical upper level. However, different applications have different goals and different trade-offs also appear due to specific aims which can be categorized as a brunch of resource allocation at the same time. IRS and UAV technologies can also contribute to and further ameliorate communication security.

Chapter 3

Literature Review

In this chapter, several newly emerged technologies pertinent to IRS and UAV are represented. The following prospects and considerations for each are also discussed and compared with the traditional IRS and UAV. There are several perspectives to evaluate those systems, such as cost, energy consumption, lifetime, complexity of construction, coverage, data transmitting speed and so on.

3.1 Active IRS-assisted system

Although the traditional IRS is formed by passive elements, it can also be active [43] by equipping with amplifiers behind every element. The purpose of the active IRS technique is to further increase the beamforming gain which is constrained by the passive element, because the passive element can only elevate the beamforming gain by adjusting the phase of the input signal. As well as the phase is optimised, the biggest gain it achieves, which may still not be enough for long-distance transmission.

Another significant advantage of using active IRS-assisted is its suppression of the double path loss effect which may cause signal distortion and reduce the signal quality at the side of the receiver. Other technologies such as Distributed Antenna Systems (DAS) and MIMO can also mitigate the double path loss effect but the complexity of those methods is even greater compared with active IRS. However, compared with the conventional IRS technology, active IRS has more power consumption and more manufacturing and deployment costs, it also requires a more precise real-time adaptation.

3.2 Self-sustainable IRS system

As mentioned in Section 2.2, the relay and the repeater are the first choices of the intermediary signal processor between the transmitter and receiver before the time of IRS. One of the advanced functions of the active relay is energy harvesting (EH), which indicates harvesting energy from several specific and preferred radio frequency (RF) resources. After harvesting the power of the signal, the relay can utilise it in many ways such as charging the battery power, processing and transmitting the signal. Nevertheless, there are many restrictions on EH relays. First of all, the harvest efficiency is between 20% and 60%, which is quite low and wastes a lot of energy. Secondly, the time to store enough inner available power by transferring the energy from the signals is also relatively long, due to the relay battery storage and the consumption energy of for processing and forwarding the signal. At last, most relays are only capable of half-duplex (HD) communication, which significantly makes the two former issues worse. As for full-duplex (FD) relays, the signal interference by their own antennas becomes another problem that cannot be ignored and the price of FD relays is normally higher than HD relays.

The IRS self-sustainable systems [44] category covers the least power-consuming IRS systems, which can harvest power from RF by applying the SWIPT technique. By combining the IRS, the difficulties such as low energy transfer efficiency, and long energy transfer time can be overcome. Furthermore, this kind of self-sustainable system is absolutely in line with the idea of green communication. The weak spots are the fees to build the self-sustainable IRS system and the complexity of designing the whole system. At the same time, the related systems are sensitive to weather conditions, which can influence the energy harvesting capabilities to a large extent.

3.3 Simultaneously transmitting and reflecting (STAR) RIS assisted system

As noted in Section 2.2, the traditional IRS technology is one panel fully equipped with passive elements that can reflect the incident signals. To fully achieve the goal of reflecting signals, one constraint is that the transmitters and the receivers must be on the same side of those passive elements, which is a 180° half-space coverage.

In order to broaden the reflecting range, the concept of Simultaneously Transmitting and

Reflecting (STAR) RIS Assisted Systems [45] is proposed. By manipulating both electric and magnetic currents, STAR-RIS's elements can achieve simultaneous transmission and reflection. Unlike the conventional IRS which can only reflect the incident signal, STAR-IRS can reflect the impact signals from the first half-space and transmit them to another half-space at the same time. This essential improvement enables STAR-IRS to gain a 360° full-space coverage which further results in multiple new design schemes for a larger Degrees-of-Freedom (DoF) leading to increasing application flexibility. For example, STAR-IRS can be adapted in Non-orthogonal Multiple Access (NOMA) nwtworks [46], STAR-RIS-NOMA systems have better performance and larger capacity and can be seen as an optimisation signal transmission technique for the existing buildings.

3.4 UAV secure network

The UAV secure network [47] is much more flexible than the secure networks on the ground since all the communication paths in the sky are LOS without any barriers, this condition also leads to a higher data rate which improves the security at the same time. Due to its mobility feature the formation of UAVs varies which gives the UAV extensive coverage and a lot of adjusting space. Those two advantages greatly strengthen the fault tolerance of the system and also help legitimate users to face threats and attacks from hackers. The algorithm design for UAV secure networks also has a wide scope for development, and that's what most of the telecommunication scholars are dedicating to. Since UAVs use a lot of embedded technologies, there is a lot of room for improvement at the electrical hardware level too.

However, the expenditure to produce UAVs and extra overhead for maintenance are quite huge, and the energy consumption for the flying network is significant as well. Meanwhile, the UAV can be affected by severe weather easily. Concurrently, the UAV can also be targeted by the eavesdropper simply which causes additional security enhancement for the UAV. It is very controversial to judge the performance of the UAV secure network because the UAVs can improve the communication quality of the users and it can be bugged since its accompanying leakage channels are LoS dominated likewise. Most uncertainties of UAV secure network are originally brought by the PLS.

New Technology	Advantage	Disadvantage
Active IRS-assisted system	• bigger beamforming gain • less double path loss effect • less complex than relay	• more precise real-time adaptation • more power consumption
Self-sustainable IRS system	• longer lifetime • less energy consumption • higher energy transfer efficiency • closer green communications concept • less EH time	• more complexity • much more cost • more sensitive to weather
STAR-RIS	• much more coverage up to full-space • more system designs • more application flexibility • more compatible for existing buildings	• much more complexity • much more cost
UAV secure network	• larger coverage • higher data rate • more flexibility • more secure for the user	• more expense • more frequent maintenance • more dependent on weather • more leakage from UAV • much more energy consumption

Figure 3.1: Summary of the Literature View

Chapter 4

Preliminary Work

In the last chapter, several different scenarios and deliverables of IRS and UAV technologies are introduced and compared, and the goal of this chapter is to search for the 'missing part' among those pieces of literature. From the existing documents, one of the missing points is the extension of the UAV-assisted IRS secure system for future city development with multi-layer structures. Thus, the aim of this thesis is beamforming design for secure networks by combining the IRS and UAV technology and it can be categorised as an improvement in safety and flexibility in the IRS system.

All the beamforming design technical terms and contents start in this chapter, a specific system model is designed with details such as the components within the system, the impact of the position of the UAV and the expected deliverables and standards to evaluate the performance of the system. Additionally, a problem formulation is created to further describe the system and more importantly, to set the standards to assess the system's effectiveness. More details will be illustrated after this chapter, such as the convexity analysis [31] of the problem formulation and the final algorithm design to solve it. The system model determines the problem formulation directly and later influences the convexity indirectly. The simulation result can give slightly distinct feedback to the designed algorithm and reveal the performance of this UAV-assisted IRS system. Chapter 3,4,5,6 are highly related to each other and they are performed to reflect the main issue and focus of this thesis step by step. Figure 4.1 briefly shows the main design procedure for the whole project.

This chapter is dedicated to providing a system model with the following problem formulation, which aims to describe an IRS-assisted secure system with a UAV and explain the fundamental concept and logic used to improve the system's performance. The sum secrecy

rate [39] is the standard to evaluate the secure performance of the whole system which is generally affected by the signals transmitted from BS, the IRS, the UAV, and the number of selected users to sacrifice.

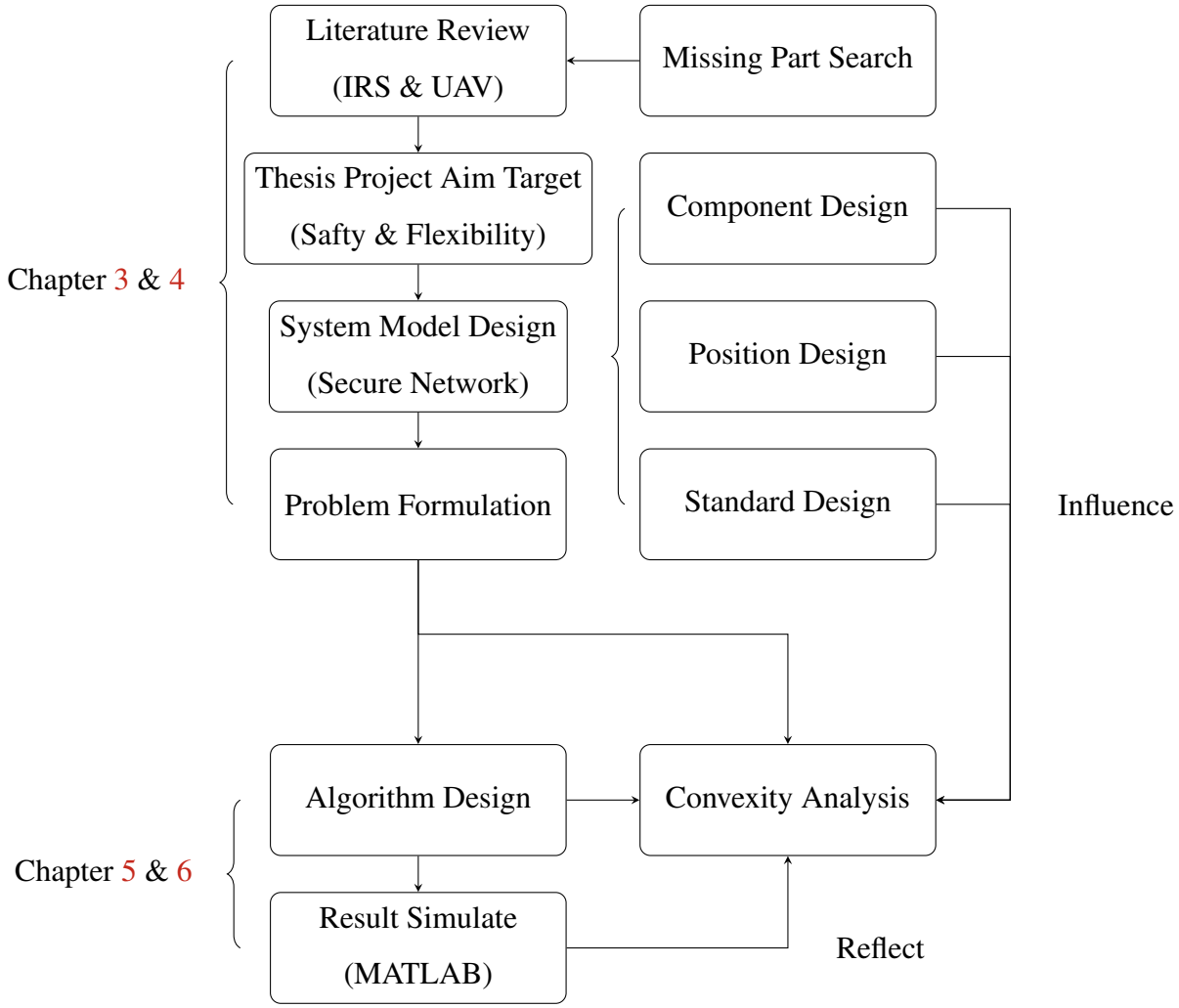

Figure 4.1: Project design flowchart

4.1 System model

There are a number of different subjects within the network. Assuming that the CSI is perfectly known. Besides, all channels in this system are considered to experience frequency flat Rician fading with an altitude-dependent Rician factor and Gaussian noise $n \sim \mathcal{CN}(\mu, \sigma^2)$.

Within the designed network, there are $\mathcal{L}$ = (1, 2, ... , L) Legitimate users (LU) and $\mathcal{M}$ = (1, 2, ... , M) Eavesdroppers (ED). Noticeably, there are $\mathcal{D}$ = (1, 2, ... , D) Selected Users

(SU) from the LU group, in addition, SU is the LU who has a lower Signal-to-Interference-Plus-Noise Ratio (SINR) than one specific value γ_{min}. Their positions can be represented by a coordinate system for which $(x_i, y_i, 0)$ represents the ith LU and $(x_j, y_j, 0)$ stands for the jth ED where $i \in \mathcal{L}$ and $j \in \mathcal{M}$.

One BS with N_T antennas is located at $(x_t, y_t, 0)$ and can generate information signals and artificial noise at the same time, which is given by

$$\mathbf{x} = \sum_{i \in \mathcal{L}} \mathbf{w}_i s_i + \mathbf{a}, \ \forall i \in \mathcal{L}, \tag{1}$$

where $\mathbf{x}$ means the transmitted signal from BS within one coherence time period, $\mathbf{w}_i \in \mathbb{C}^{N_T \times 1}$ and $s_i \in \mathbb{C}$ are the beamforming vector and information signal for the ith LU, $\mathbf{a} \in \mathbb{C}^{N_T \times 1}$ is the artificial noise vector. It is obvious that the summation power of signals and artificial noise generated from BS should be smaller than the maximum generating power P_{BS}, which is given by

$$\sum_{i \in \mathcal{L}} \|\mathbf{w}_i\|^2 + \|\mathbf{a}\|^2 \leq P_{BS}, \ \forall i \in \mathcal{L}, \tag{2}$$

One UAV-assisted IRS is sited at (x_u, y_u, z), where

$$\mathcal{Z}_{min} \leq z \leq \mathcal{Z}_{max}, \tag{3}$$

and x_u, y_u is fixed. There are N passive reflecting elements on IRS and the reflection coefficient matrix of IRS can be noted as a diagonal matrix

$$\Phi \triangleq \text{diag}\left(\left[e^{j\theta_1}, e^{j\theta_2}, \ldots, e^{j\theta_N}\right]\right) \in \mathbb{C}^{N \times N}, \tag{4}$$

where θ_n, $\forall n \in N$ notes the phase shift of the nth reflector of the IRS panel. All the components within this system are listed in Figure 4.2.

There are five straight links existing in the network, the channel between BS and IRS H, the link between BS and LUs h_d^H, the channel between BS and EDs h_r^H, the link between IRS and LUs g_d^H and the path between IRS and EDs g_r^H. Assuming that the straight links between BS and LUs h_d^H, EDs g_d^H are all NLOS. Besides, the attenuation function is defined as $\beta(z)$ as a function of the distance between the UAV-assisted IRS and the LUs and EDs. It can be calculated by the Euclidean distance in the defined coordinate system by using the coordinate of the UAV (x_u, y_u, z) and the coordinate of the ith LU $(x_i, y_i, 0)$ or the jth ED $(x_j, y_j, 0)$. $\beta_i(z)$ and $\beta_j(z)$ are separately calculated as

$$\beta_i(z) = \frac{1}{(x_u - x_i)^2 + (y_u - y_i)^2 + z^2}, \tag{5.1}$$

Components	Quantity
BS (antenna number)	1 (N_T)
UAV (horizontal coordinates, height)	1 (x_u, y_u, z)
IRS (element number)	1 (N)
Legitimate User (LU)	$\mathcal{L}$
Eavesdroppers (ED)	$\mathcal{M}$
Selected User (SU)	$\mathcal{D}$

Figure 4.2: System Components

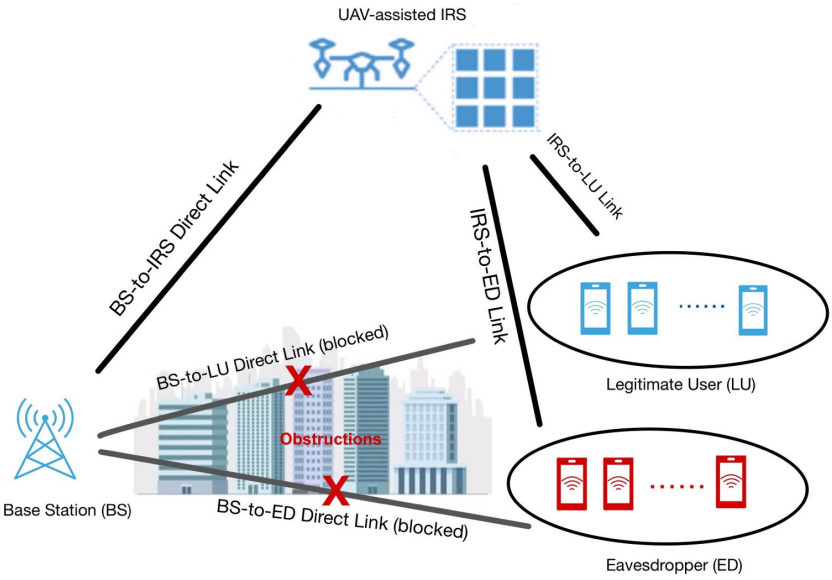

Figure 4.3: System Model

$$\beta_j(z) = \frac{1}{(x_u - x_j)^2 + (y_u - y_j)^2 + z^2}. \tag{5.2}$$

The System Model is shown in Figure 4.3.

4.2 Problem formulation

The received signal at the ith LU can be represented as

$$\begin{aligned} y_i = & \underbrace{\mathbf{h}_{d,i}^H \mathbf{x}}_{\text{direct link (blocked)}} + \underbrace{\sqrt{\beta_{i,out}} \mathbf{h}_{r,i}^H \Phi \mathbf{H} \mathbf{x} \sqrt{\beta_{i,in}}}_{\text{reflected link}} + n_i \\ \triangleq & \sqrt{\beta_{i,out}\beta_{i,in}} \mathbf{h}_i^H \Phi \mathbf{H} \mathbf{x} + n_i \\ = & \sqrt{\beta_{i,out}\beta_{i,in}} \mathbf{h}_i^H \Phi \mathbf{H} (\sum_{i \in \mathcal{L}} \mathbf{w}_i s_i + \mathbf{a}) + n_i \\ \triangleq & \sqrt{\beta_i} \mathbf{h}_i^H \Phi \mathbf{H} (\sum_{i \in \mathcal{L}} \mathbf{w}_i s_i + \mathbf{a}) + n_i, \ \forall i \in \mathcal{L}. \end{aligned} \tag{6}$$

The SINR at the ith LU

$$\text{SINR}_i = \frac{\beta_i \left| \mathbf{h}_i^H \Phi \mathbf{H} \mathbf{w}_i \right|^2}{\sum\limits_{k \in \mathcal{L} \setminus \{i\}} \beta_i \left| \mathbf{h}_i^H \Phi \mathbf{H} \mathbf{w}_k \right|^2 + \beta_i \left| \mathbf{h}_i^H \Phi \mathbf{H} \mathbf{a} \right|^2 + \sigma_i^2}, \ \forall i \in \mathcal{L}. \tag{7}$$

The achievable rate for the ith LU

$$R_i = \log_2 (1 + SINR_i), \quad \forall i \in \mathcal{L}. \tag{8}$$

Similarly, from the point of view of the jth ED attempts to decode the signal $\mathbf{w}_i$ sent to the ith LU, the equation becomes

$$\begin{aligned} y_j = & \underbrace{\mathbf{g}_{d,j}^H x}_{\text{direct link (blocked)}} + \underbrace{\sqrt{\beta_{j,out}} \mathbf{g}_{r,j}^H \Phi \mathbf{H} x \sqrt{\beta_{j,in}}}_{\text{reflected link}} + n_j \\ \triangleq & \sqrt{\beta_{j,out}\beta_{j,in}} \mathbf{g}_j^H \Phi \mathbf{H} \mathbf{x} + n_j \\ = & \sqrt{\beta_{j,out}\beta_{j,in}} \mathbf{g}_j^H \Phi \mathbf{H} (\sum_{i \in \mathcal{L}} \mathbf{w}_i s_i + \mathbf{a}) + n_j \\ \triangleq & \sqrt{\beta_j} \mathbf{g}_j^H \Phi \mathbf{H} (\sum_{i \in \mathcal{L}} \mathbf{w}_i s_i + \mathbf{a}) + n_j, \quad \forall j \in \mathcal{M}. \end{aligned} \tag{9}$$

The SINR at the jth ED wiretapping ith LU

$$\text{SINR}_{j,i} = \frac{\beta_j \left| \mathbf{g}_j^H \Phi \mathbf{H} \mathbf{w}_i \right|^2}{\sum\limits_{k \in \mathcal{L} \setminus \{i\}} \beta_j \left| \mathbf{g}_j^H \Phi \mathbf{H} \mathbf{w}_k \right|^2 + \beta_j \left| \mathbf{g}_j^H \Phi \mathbf{H} \mathbf{a} \right|^2 + \sigma_j^2}, \quad \forall j \in \mathcal{M}. \tag{10}$$

The achievable rate for the jth ED spying on ith LU

$$R_{j,i} = \log_2 \left(1 + SINR_{j,i}\right), \quad \forall j \in \mathcal{M}, \quad \forall i \in \mathcal{L}. \tag{11}$$

Assuming that every ED can spy on all the LUs, but the secrecy rate of the ith LU only takes the ED who wiretaps most information from this user into consideration and ignores other EDs who eavesdrop not much information. Accordingly, the secrecy rate of the ith LU can be written as

$$R_{d,i} = \left[R_i - \max_{j \in \mathcal{M}} R_{j,i} \right]^+, \ \forall i \in \mathcal{L}, \tag{12}$$

where $[\cdot]^+$ denotes the positive part of a mathematical expression. It's used to extract the non-negative portion of a number while discarding the negative part.

One key principle of increasing the sum secrecy rate of LUs is to select some LUs to sacrifice, which means ignoring some LUs that have a diminutive SINR value. LUs with SINR values lower than γ_{min} will be chosen as SUs, and the BS will stop sending information signals to those selected ones. Therefore, the saved resource can be allocated to other LUs and improve the sum secrecy rate of the whole network. Consequently, a selecting parameter and also the binary variable d_i for selecting the sacrificed users is defined as

$$d_i = \begin{cases} 0, & \text{if } SINR_i \leq \gamma_{min}, \\ 1, & \text{if } SINR_i > \gamma_{min}. \end{cases} \tag{13}$$

After applying this method, the equation 2 and 12 can be written as

$$\sum_{i \in \mathcal{L}} d_i \|\mathbf{w}_i\|^2 + \|\mathbf{a}\|^2 \leq P_{\text{BS}}, \ \forall i \in \mathcal{L}, \tag{14}$$

and

$$R_{d,i} = d_i \left[R_i - \max_{j \in \mathcal{M}} R_{j,i} \right]^+, \ \forall i \in \mathcal{L}, \quad d_i \in \{0,1\}. \tag{15}$$

Moreover, there should be a limitation on the total number of SDs since it's unrealistic and unsystematic to abandon a very large portion of users. This discipline can be expressed as

$$0 \leq \mathcal{D} \leq \mathcal{D}_{max}. \tag{16}$$

Finally, the sum secrecy rate $\sum_{i \in \mathcal{L}} R_{d,i}$ is used to be the system performance evaluating stan-

dard and the corresponding optimization problem is formulated as

$$
\begin{aligned}
(\mathrm{P0}): \underset{\mathbf{w}_i,\mathbf{a}\in\mathbb{C}^{N_\mathrm{T}\times 1},\boldsymbol{\Phi},z,d_i}{\text{maximize}} \; & \sum_{i\in\mathcal{L}} R_{d,i} \\
\text{s.t..} \quad & \mathrm{C1}: \sum_{i\in\mathcal{L}} d_i\|\mathbf{w}_i\|^2 + \|\mathbf{a}\|^2 \leq P_{\mathrm{BS}}, \\
& \mathrm{C2}: \mathcal{Z}_{min} \leq z \leq \mathcal{Z}_{max}, \\
& \mathrm{C3}: |[\Phi]_{n,n}| = 1, \forall n, \\
& \mathrm{C4}: 0 \leq \mathcal{D} \leq \mathcal{D}_{max}, \\
& \mathrm{C5}: SINR_i \geq d_i\gamma_{min}, \; \forall i, \\
& \mathrm{C6}: d_i \in \{0,1\}, \; \forall i.
\end{aligned} \tag{17}
$$

Chapter 5

Solutions

It is widely acknowledged that the geometry of the problem formulation remains fixed once all the system parameters and constraints are made rigid, as briefly mentioned in Chapter 4. Besides, it's important to analyse and understand every equation's convexity or non-convexity because related efficient solutions can be found based on the geometry type of the equation. Even if some equations are both convex or non-convex, there will still be differences in the approach to solutions.

5.1 Convexity analysis

As for equation 5.1 and 5.2, it is distinct that $\beta(z)$ is a function of z and proportional to $1/z^2$, and it is convex since $z > 0$. Concerning equation 6, the main concentration is allocated to the right-hand side which is: $\sqrt{\beta_{i,out}\beta_{i,in}}\mathbf{h}_i^H\Phi\mathbf{H}\mathbf{x}+n_i$. It's still a convex function since the sum operation introduced by $\mathbf{x}$ won't change the convexity of the affine functions $\sqrt{\beta_{i,out}\beta_{i,in}}\mathbf{h}_i^H\Phi\mathbf{H}$ in this case. In addition, n_i is the Gaussian noise and can be seen as a constant. The non-convexity of the SINR primarily arises from the presence of the division operation.

With regard to the SINR at the ith LU which is noted by equation 7, there are different polynomial parts for both numerator and denominator. $\beta_i\left|\mathbf{h}_i^H\Phi\mathbf{H}\mathbf{w}_i\right|^2$ and $\sum_{k\in\mathcal{L}\setminus\{i\}}\beta_i\left|\mathbf{h}_i^H\Phi\mathbf{H}\mathbf{w}_k\right|^2+\beta_i\left|\mathbf{h}_i^H\Phi\mathbf{H}\mathbf{a}\right|^2+\sigma_i^2$. In order to analyze the convexity, both the numerator and denominator should be evaluated separately, and then the whole fraction should be taken into consideration. The numerator contains the complex conjugate operation and also the norm operation, which are the convex operations and this portion is convex. However, the denominator is not neces-

sarily convex, because the set of $\sum_{k\in\mathcal{L}\setminus\{i\}} \beta_i \left|\mathbf{h}_i^H \Phi \mathbf{H} \mathbf{w}_k\right|^2$ doesn't cover all the elements inside $\mathcal{L}$ which may cause non-convexity. More importantly, the non-convexity of the SINR primarily arises from the presence of the division operation.

In terms of the achievable rate for the ith LU R_i, it's non-convex since the inner component $SINR$ of the logarithm function is non-convex and the logarithm function is a concave function which won't affect the non-convexity. Similar to R_i, the secrecy rate of the ith LU $R_{j,i}$ is also non-convex.

In reference to the final part of the problem formulation, which is the sum secrecy rate $\sum_{i\in\mathcal{L}} d_i \left[R_i - \max_{j\in\mathcal{M}} R_{j,i}\right]^+$. It is straightforward that the sum secrecy rate expression is non-convex due to the binary variable d_i and the non-convex elements R_i and $R_{j,i}$. In addition, the subtraction between R_i and $R_{j,i}$ and the maximal operator of $R_{j,i}$ also strengthen non-convexity.

5.2 Algorithm design

Based on the convexity analysis of every part of the problem formulation, the following algorithm can be designed step by step. First of all, there are primarily five variables $\{\mathbf{w}_i\}, \{\mathbf{a}\}, \Phi, z$, and d_i and it is extremely sophisticated to solve the non-convex problem with five variables at once. Therefore, four methods namely Alternating Optimization (AO) [48], Successive Convex Approximation (SCA) [49], Semidefinite Relaxation (SDR) [50] and Oblique Manifold Optimization (OMO) [51] are applied to tackle the formulated non-convex problem.

The dedicated algorithm has four subproblems in total and each subproblem has fewer constraints compared with the problems in the upper layer. Besides, relevant methods are cited for each subproblem. For instance, Subproblem 1 assumes that the height of z is a stationary value and the SCA technique is applied to adjust the value of z, which greatly simplifies the original non-convex problem by increasing the computing times. Similarly, Subproblem 2 sets a fixed value for d_i which eliminates the constraints introduced by d_i. Subproblem 3 and Subproblem 4 are at the same level and will be solved by SCA, SDR and OMO separately under the AO Iteration frame. Noticeably, although the format of the problem formulation varies through the transformation, the reflected system model and the final goal still remain the same. The flowchart of the designed algorithm is visualized in Figure 4.1.

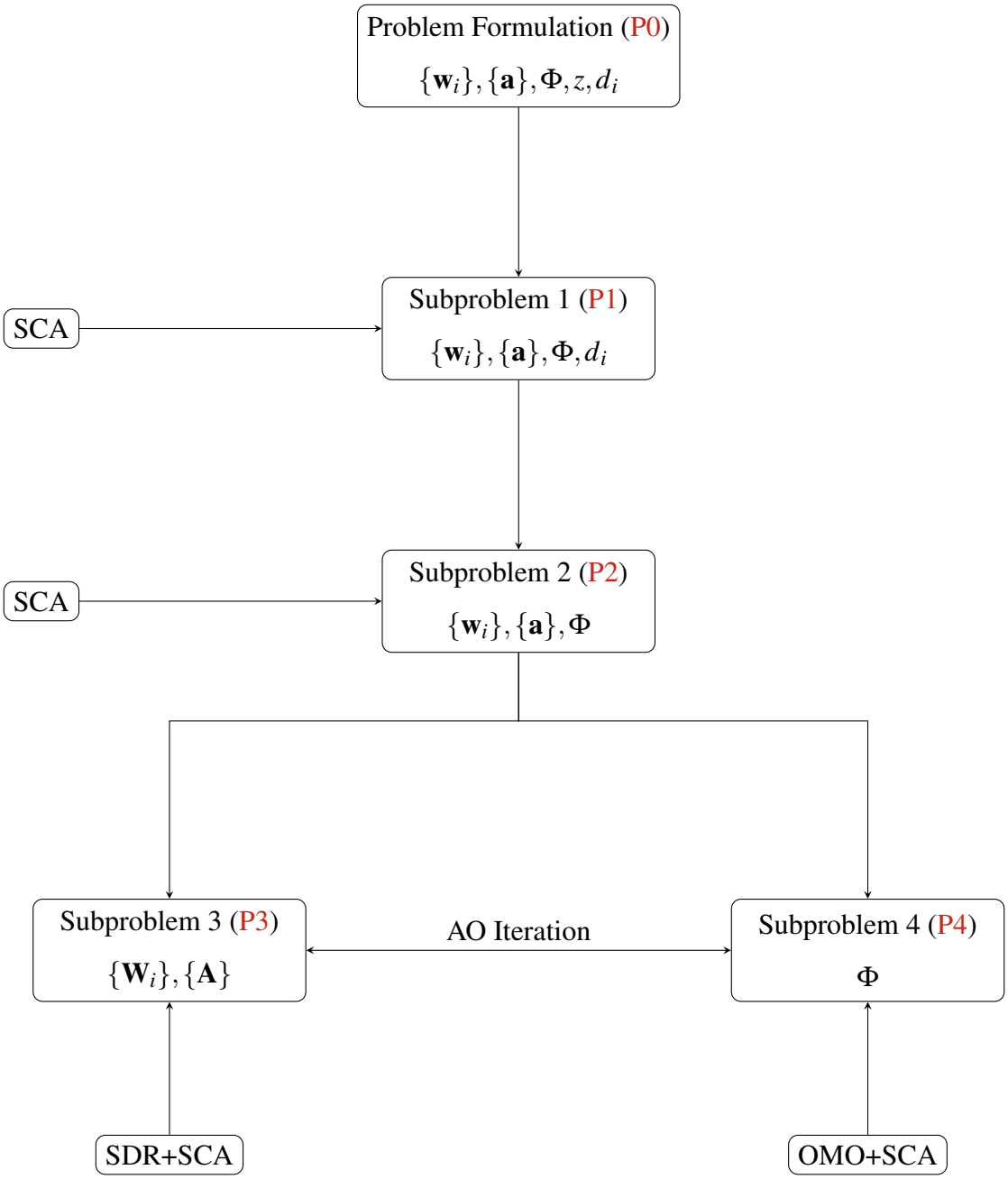

Figure 5.1: Designed structure of algorithm

5.2.1 Subproblem 1

Since d_i is the binary variable and the total number of SU is limited, based on equation 13 and equation 16, C4 can be rewritten as

$$\text{C4}' : 0 \leq \sum_{i \in \mathcal{L}} d_i \leq \mathcal{D}_{max}, \tag{18}$$

and C6 can be replaced equivalently by two equation jointly

$$\begin{aligned} &\text{C6a} : d_i - d_i^2 \leq 0, \forall i, \\ &\text{C6b} : 0 \leq d_i \leq 1, \forall i. \end{aligned} \tag{19}$$

Additionally, the height constraint C2 of P1 can be neglected due to the fact that z is seen as a steady value during every loop of SCA, which can be marked as the first loop of the whole algorithm frame. P1 can be substituted by P2

$$\begin{aligned} (\text{P1}) : \underset{\mathbf{w}_i, \mathbf{a} \in \mathbb{C}^{N_\text{T} \times 1}, \Phi, d_i}{\text{maximize}} \quad & \sum_{i \in \mathcal{L}} R_{d,i} \\ \text{s.t..} \quad & \text{C1} : \sum_{i \in \mathcal{L}} d_i \|\mathbf{w}_i\|^2 + \|\mathbf{a}\|^2 \leq P_\text{BS}, \\ & \cancel{\text{C2} : \mathcal{Z}_{min} \leq z \leq \mathcal{Z}_{max},} \\ & \text{C3} : |[\Phi]_{n,n}| = 1, \forall n, \\ & \text{C4}' : 0 \leq \sum_{i \in \mathcal{L}} d_i \leq \mathcal{D}_{max}, \\ & \text{C5} : SINR_i \geq d_i \gamma_{min}, \ \forall i, \\ & \text{C6a} : d_i - d_i^2 \leq 0, \forall i, \\ & \text{C6b} : 0 \leq d_i \leq 1, \forall i. \end{aligned} \tag{20}$$

5.2.2 Subproblem 2

In the vein of Subproblem 1, d_i is fixed during the second loop of SCA, which removes the constraints like C4', C6a and C6b that are related to this binary variable. In the end, Subproblem 2

can be refined as

$$
\begin{aligned}
(\mathrm{P2}):\ \underset{\mathbf{w}_i,\mathbf{a}\in\mathbb{C}^{N_T\times 1},\Phi}{\text{maximize}}\ & \sum_{i\in\mathcal{L}} R_{d,i} \\
\text{s.t..}\quad & \mathrm{C1}:\ \sum_{i\in\mathcal{L}} d_i\|\mathbf{w}_i\|^2 + \|\mathbf{a}\|^2 \le P_{\mathrm{BS}}, \\
& \cancel{\mathrm{C2}:\ \mathcal{Z}_{min} \le z \le \mathcal{Z}_{max},} \\
& \mathrm{C3}:\ |[\Phi]_{n,n}| = 1, \forall n, \\
& \cancel{\mathrm{C4}':\ 0 \le \sum_{i\in\mathcal{L}} d_i \le \mathcal{D}_{max},} \\
& \mathrm{C5}:\ SINR_i \ge d_i\gamma_{min},\ \forall i, \\
& \cancel{\mathrm{C6a}:\ d_i - d_i^2 \le 0, \forall i,} \\
& \cancel{\mathrm{C6b}:\ 0 \le d_i \le 1, \forall i.}
\end{aligned} \tag{21}
$$

5.2.3 Subproblem 3

In order to find the optimal solution for Subproblem 2, the AO algorithm is used to separate the effect of variables $\mathbf{w}_i, \mathbf{a}$ and Φ. Under this circumstance, both SCA and SDR techniques are applied to Subproblem 3. For notational simplicity, new notations are defined as $\mathbf{P}_i = \mathrm{diag}(\mathbf{h}_i^H)\mathbf{H}$, $\mathbf{G}_j$=diag$(\mathbf{g}_j^H)\mathbf{H}$, $\mathbf{W}_i = \mathbf{w}_i\mathbf{w}_i^H$. New constraints such as Rank$(\mathbf{W}_i) \le 1$ and $\mathbf{W_i} \succeq \mathbf{0}$ are applied to maintain perfect equality. The covariance matrix $\mathbf{A} \in \mathbb{H}^{N_T\times 1}$ of the artificial noise vector $\mathbf{a}$ is also introduced to substitute $\mathbf{a}$, which brings another constraint $\mathbf{A} \succeq \mathbf{0}$. Moreover, a new optimization variable $\mathbf{u} = \left[e^{j\theta_1}, e^{j\theta_2}, \ldots, e^{j\theta_N}\right]^T$ is defined to represent the physical meaning of Φ.

Then, the SINR at the ith LU can be rewritten as

$$
\mathrm{SINR}_i = \frac{\beta_i \mathrm{Tr}\left(\mathbf{W}_i\mathbf{P}_i^H\mathbf{u}\mathbf{u}^H\mathbf{P}_i\right)}{\sum\limits_{k\in\mathcal{L}\setminus\{i\}} \beta_i \mathrm{Tr}\left(\mathbf{W}_k\mathbf{P}_i^H\mathbf{u}\mathbf{u}^H\mathbf{P}_i\right) + \beta_i \mathrm{Tr}\left(\mathbf{A}\mathbf{P}_i^H\mathbf{u}\mathbf{u}^H\mathbf{P}_i\right) + \sigma_i^2},\ \forall i \in \mathcal{L}. \tag{22}
$$

The achievable rate for the ith LU can be rewritten as

$$
\begin{aligned}
R_i &= \log_2\left(1 + \frac{\beta_i \mathrm{Tr}\left(\mathbf{W}_i\mathbf{P}_i^H\mathbf{u}\mathbf{u}^H\mathbf{P}_i\right)}{\sum\limits_{k\in\mathcal{L}\setminus\{i\}} \beta_k \mathrm{Tr}\left(\mathbf{W}_k\mathbf{P}_i^H\mathbf{u}\mathbf{u}^H\mathbf{P}_i\right) + \beta_i \mathrm{Tr}\left(\mathbf{A}\mathbf{P}_i^H\mathbf{u}\mathbf{u}^H\mathbf{P}_i\right) + \sigma_i^2}\right) \\
&= \log_2\left(\frac{\sum\limits_{k\in\mathcal{L}} \beta_i \mathrm{Tr}\left(\mathbf{W}_k\mathbf{P}_i^H\mathbf{u}\mathbf{u}^H\mathbf{P}_i\right) + \beta_i \mathrm{Tr}\left(\mathbf{A}\mathbf{P}_i^H\mathbf{u}\mathbf{u}^H\mathbf{P}_i\right) + \sigma_i^2}{\sum\limits_{k\in\mathcal{L}\setminus\{i\}} \beta_i \mathrm{Tr}\left(\mathbf{W}_k\mathbf{P}_i^H\mathbf{u}\mathbf{u}^H\mathbf{P}_i\right) + \beta_i \mathrm{Tr}\left(\mathbf{A}\mathbf{P}_i^H\mathbf{u}\mathbf{u}^H\mathbf{P}_i\right) + \sigma_i^2}\right) \\
&\triangleq B_1 - F_1, \quad \forall i,
\end{aligned} \tag{23}
$$

where

$$B_1 = \log_2\left(\sum_{k\in\mathcal{L}} \beta_i \operatorname{Tr}\left(\mathbf{W}_k \mathbf{P}_i^H \mathbf{u}\mathbf{u}^H \mathbf{P}_i\right) + \beta_i \operatorname{Tr}\left(\mathbf{A}\mathbf{P}_i^H \mathbf{u}\mathbf{u}^H \mathbf{P}_i\right) + \sigma_i^2\right) \tag{24}$$

and

$$F_1 = \log_2\left(\sum_{k\in\mathcal{L}\setminus\{i\}} \beta_i \operatorname{Tr}\left(\mathbf{W}_k \mathbf{P}_i^H \mathbf{u}\mathbf{u}^H \mathbf{P}_i\right) + \beta_i \operatorname{Tr}\left(\mathbf{A}\mathbf{P}_i^H \mathbf{u}\mathbf{u}^H \mathbf{P}_i\right) + \sigma_i^2\right). \tag{25}$$

The SINR at the jth ED wiretapping ith LU can be rewritten as

$$\mathrm{SINR}_{j,i} = \frac{\beta_j \operatorname{Tr}\left(\mathbf{W}_i \mathbf{G}_j^H \mathbf{u}\mathbf{u}^H \mathbf{G}_j\right)}{\sum\limits_{k\in\mathcal{L}\setminus\{i\}} \beta_j \operatorname{Tr}\left(\mathbf{W}_k \mathbf{G}_j^H \mathbf{u}\mathbf{u}^H \mathbf{G}_j\right) + \beta_j \operatorname{Tr}\left(\mathbf{A}\mathbf{G}_j^H \mathbf{u}\mathbf{u}^H \mathbf{G}_j\right) + \sigma_j^2}, \quad j \in \mathcal{M}, \tag{26}$$

The achievable rate for the jth ED spying on ith LU can be rewritten as

$$\begin{aligned} R_{j,i} &= \log_2\left(1 + \frac{\beta_j \operatorname{Tr}\left(\mathbf{W}_i \mathbf{G}_j^H \mathbf{u}\mathbf{u}^H \mathbf{G}_j\right)}{\sum\limits_{k\in\mathcal{L}\setminus\{i\}} \beta_j \operatorname{Tr}\left(\mathbf{W}_k \mathbf{G}_j^H \mathbf{u}\mathbf{u}^H \mathbf{G}_j\right) + \beta_j \operatorname{Tr}\left(\mathbf{A}\mathbf{G}_j^H \mathbf{u}\mathbf{u}^H \mathbf{G}_j\right) + \sigma_j^2}\right) \\ &= \log_2\left(\frac{\sum\limits_{k\in\mathcal{L}} \beta_j \operatorname{Tr}\left(\mathbf{W}_i \mathbf{G}_j^H \mathbf{u}\mathbf{u}^H \mathbf{G}_j\right) + \beta_j \operatorname{Tr}\left(\mathbf{A}\mathbf{G}_j^H \mathbf{u}\mathbf{u}^H \mathbf{G}_j\right) + \sigma_j^2}{\sum\limits_{k\in\mathcal{L}\setminus\{i\}} \beta_j \operatorname{Tr}\left(\mathbf{W}_k \mathbf{G}_j^H \mathbf{u}\mathbf{u}^H \mathbf{G}_j\right) + \beta_j \operatorname{Tr}\left(\mathbf{A}\mathbf{G}_j^H \mathbf{u}\mathbf{u}^H \mathbf{G}_j\right) + \sigma_j^2}\right) \\ &\triangleq F_2 - B_2, \quad \forall j, \quad \forall i, \end{aligned} \tag{27}$$

where

$$F_2 = \log_2\left(\sum_{k\in\mathcal{L}} \beta_j \operatorname{Tr}\left(\mathbf{W}_i \mathbf{G}_j^H \mathbf{u}\mathbf{u}^H \mathbf{G}_j\right) + \beta_j \operatorname{Tr}\left(\mathbf{A}\mathbf{G}_j^H \mathbf{u}\mathbf{u}^H \mathbf{G}_j\right) + \sigma_j^2\right) \tag{28}$$

and

$$B_2 = \log_2\left(\sum_{k\in\mathcal{L}\setminus\{i\}} \beta_j \operatorname{Tr}\left(\mathbf{W}_k \mathbf{G}_j^H \mathbf{u}\mathbf{u}^H \mathbf{G}_j\right) + \beta_j \operatorname{Tr}\left(\mathbf{A}\mathbf{G}_j^H \mathbf{u}\mathbf{u}^H \mathbf{G}_j\right) + \sigma_j^2\right). \tag{29}$$

Finally, the secrecy rate of the ith LU can be rewritten as

$$\begin{aligned} R_{d,i} &= d_i \left[R_i - \max_{j\in M} R_{j,i}\right]^+ \\ &= d_i \min_{j\in M} \left[R_i - R_{j,i}\right]^+ \\ &= \min_{j\in M} d_i \left[R_i - R_{j,i}\right]^+ \\ &= \min_{j\in M} d_i \left[B_1 - F_1 - F_2 + B_2\right]^+, \quad \forall i \in \mathcal{L}, \quad \forall j \in \mathcal{M}, \quad d_i \in \{0,1\}. \end{aligned} \tag{30}$$

It is obvious that the operator $[\cdot]^+$ won't affect the optimal solution which can be neglected.

At last, Subproblem 3 can be expressed as

$$
\begin{aligned}
\text{(P3)}: \underset{\mathbf{W}_i,\mathbf{A}}{\text{maximize}} \quad & \sum_{i\in\mathcal{L}} \tau_i \\
\text{s.t..} \quad & \text{C1}': \sum_{i\in\mathcal{L}} d_i \text{Tr}\left(\mathbf{W}_i\right) + \text{Tr}\left(\mathbf{A}\right) \le P_{\text{BS}}, \\
& \cancel{\text{C2}: \mathcal{Z}_{min} \le z \le \mathcal{Z}_{max},} \\
& \cancel{\text{C3}': |u_n| = 1, \forall n,} \\
& \cancel{\text{C4}: 0 \le \sum_{i\in\mathcal{L}} d_i \le \mathcal{D}_{max},} \\
& \text{C5}': \beta_i \text{Tr}\left(\mathbf{W}_i \mathbf{P}_i^H \mathbf{u}\mathbf{u}^H \mathbf{P}_i\right) - d_i \gamma_{min} \sum_{k\in\mathcal{L}\setminus\{i\}} \beta_i \text{Tr}\left(\mathbf{W}_k \mathbf{P}_i^H \mathbf{u}\mathbf{u}^H \mathbf{P}_i\right) \\
& \qquad - d_i \gamma_{min} \beta_i \text{Tr}\left(\mathbf{A}\mathbf{P}_i^H \mathbf{u}\mathbf{u}^H \mathbf{P}_i\right) - d_i \gamma_{min} \sigma_i^2 \ge 0, \ \forall i, \\
& \cancel{\text{C6a}: d_i - d_i^2 \le 0, \forall i,} \\
& \cancel{\text{C6b}: 0 \le d_i \le 1, \forall i,} \\
& \text{C7}: \mathbf{A} \succeq \mathbf{0}, \\
& \text{C8}: \text{Rank}\left(\mathbf{W}_i\right) \le 1, \forall i, \\
& \text{C9}: \mathbf{W_i} \succeq \mathbf{0}, \forall i, \\
& \text{C10}: \tau_i \le \ d_i \left(B_1 + B_2 - F_1 - F_2\right). \qquad (31)
\end{aligned}
$$

It is obvious that constrain C10 $\tau_i \le \ d_i \left(\underbrace{B_1}_{\text{concave}} \ \underbrace{+B_2}_{\text{concave}} \ \underbrace{-F_1}_{\text{convex}} \ \underbrace{-F_2}_{\text{convex}} \right)$ is still non-convex, which leads to the following SCA and SDR techniques.

Furthermore, for any feasible point $\mathbf{W}_i$ and $\mathbf{A}$, both the differentiable concave function $\widetilde{F}_1$ and $\widetilde{F}_2$ have global underestimators which satisfy the following inequality

$$
\begin{aligned}
F_1(\mathbf{W},\mathbf{A}) \le & F_1\left(\mathbf{W}^i,\mathbf{A}^i\right) \\
& + \text{Tr}\left(\left(\nabla_{\mathbf{W}} F_1\left(\mathbf{W}^i,\mathbf{A}^i\right)\right)^H \left(\mathbf{W}-\mathbf{W}^i\right)\right) \\
& + \text{Tr}\left(\left(\nabla_{\mathbf{A}} F_1\left(\mathbf{W}^i,\mathbf{A}^i\right)\right)^H \left(\mathbf{A}-\mathbf{A}^i\right)\right) \\
& \triangleq \widetilde{F}_1\left(\mathbf{W},\mathbf{A},\mathbf{W}^i,\mathbf{A}^i\right), \qquad (32)
\end{aligned}
$$

$$
\begin{aligned}
F_2(\mathbf{W},\mathbf{A}) \leq\ & F_2\left(\mathbf{W}^i,\mathbf{A}^i\right) \\
& + \mathrm{Tr}\left(\left(\nabla_{\mathbf{W}} F_2\left(\mathbf{W}^i,\mathbf{A}^i\right)\right)^H\left(\mathbf{W}-\mathbf{W}^i\right)\right) \\
& + \mathrm{Tr}\left(\left(\nabla_{\mathbf{A}} F_2\left(\mathbf{W}^i,\mathbf{A}^i\right)\right)^H\left(\mathbf{A}-\mathbf{A}^i\right)\right) \\
& \triangleq \widetilde{F}_2\left(\mathbf{W},\mathbf{A},\mathbf{W}^i,\mathbf{A}^i\right). \qquad (33)
\end{aligned}
$$

The problem formulation becomes

$$
\begin{aligned}
\text{(P3)}: \underset{\mathbf{W}_i,\mathbf{A}}{\text{maximize}} \quad & \sum_{i\in\mathcal{L}} \tau_i \\
\text{s.t..} \quad & \mathrm{C1}', \mathrm{C5}', \mathrm{C7}, \mathrm{C8}, \mathrm{C9}, \\
& \mathrm{C10}': \tau_i \leq\ d_i\left(B_1 + B_2 - \widetilde{F}_1 - \widetilde{F}_2\right). \qquad (34)
\end{aligned}
$$

It is very straightforward that equation 34 is still non-convex due to the rank-one constraint for C8. In order to solve the non-convexity of equation 34, the SDR technique is adapted to approximate equation 34 as a convex semidefinite program (SDP) [31], which can be solved by convex problem solvers like CVX [52]. Moreover, the tightness of SDR is revealed in the following *Theorem 1*.

*Theorem 1:*If $P_{\max} > 0$, an optimal beamforming matrix $\mathbf{W}_i$ satisfying $\mathrm{Rank}(\mathbf{W}_i) \leq 1$ can always be obtained.

*Proof:*Based on the assumption that $\mathrm{Rank}\left(\mathbf{W}_i\right) \leq 1, \forall i$, Appendix 1.

It is apparent that the constraint C10' represents a lower bound of equation 31. Algorithm 1 is a SCA-Based optimization algorithm that aims to tighten the lower bound iteratively and acquire a sequence of solutions $\mathbf{W}$ and $\mathbf{A}$. Since the objective function in equation 34 is non-decreasing in each iteration, the designed algorithm can find a locally optimal point from the whole coverage.

5.2.4 Subproblem 4

Constraints C1', C7, C8 and C9 can be further eliminated in subproblem 4 since $\mathbf{W}_i, \mathbf{A}$ are fixed within every SCA loop. Then, the optimisation problem to $\sum_{i\in\mathcal{L}} \tau_i$ becomes a problem to find the maximal value of a function that is only determined by a single variable $\mathbf{u}_n$. Subproblem 4 can be solved by SCA and OMO and can also be expressed as

Algorithm 1 SCA-Based Optimization for Subproblem 3

1: **Initialize:** Set iteration index $i = 1$, set Φ.

2: **repeat**

3: Solve P3 for given $\mathbf{W}^{(i)}$ and $\mathbf{A}^{(i)}$ and store the intermediate solution $\mathbf{W}$, $\mathbf{A}$

4: Set $i = i + 1$ and $\mathbf{W}^{(i)} = \mathbf{W}$ and $\mathbf{A}^{(i)} = \mathbf{A}$

5: **until** Convergence of P4 attained.

6: **Output:** Optimal Solution Set $\mathbf{W}^* = \mathbf{W}^{(i)}$, $\mathbf{A}^* = \mathbf{A}^{(i)}$.

$$
\begin{aligned}
(\text{P4}) : \underset{u_n}{\text{maximize}} \quad & \sum_{i\in\mathcal{L}} \tau_i \\
\text{s.t..} \quad & \cancel{\text{C1}' : \sum_{i\in\mathcal{L}} d_i \text{Tr}\left(\mathbf{W}_i\right) + \text{Tr}\left(\mathbf{A}\right) \leq P_{\text{BS}},} \\
& \cancel{\text{C2} : \mathcal{Z}_{min} \leq z \leq \mathcal{Z}_{max},} \\
& \text{C3}' : |u_n| = 1, \forall n, \\
& \cancel{\text{C4} : 0 \leq \sum_{i\in\mathcal{L}} d_i \leq \mathcal{D}_{max},} \\
& \text{C5}' : \beta_i \text{Tr}\left(\mathbf{W}_i \mathbf{P}_i^H \mathbf{u}\mathbf{u}^H \mathbf{P}_i\right) - d_i \gamma_{min} \sum_{k\in\mathcal{L}\setminus\{i\}} \beta_i \text{Tr}\left(\mathbf{W}_k \mathbf{P}_i^H \mathbf{u}\mathbf{u}^H \mathbf{P}_i\right) \\
& \qquad - d_i \gamma_{min} \beta_i \text{Tr}\left(\mathbf{A}\mathbf{P}_i^H \mathbf{u}\mathbf{u}^H \mathbf{P}_i\right) - d_i \gamma_{min} \sigma_i^2 \geq 0, \ \forall i, \\
& \cancel{\text{C6a} : d_i - d_i^2 \leq 0, \forall i,} \\
& \cancel{\text{C6b} : 0 \leq d_i \leq 1, \forall i,} \\
& \cancel{\text{C7} : \mathbf{A} \succeq \mathbf{0},} \\
& \cancel{\text{C8} : \text{Rank}\left(\mathbf{W}_i\right) \leq 1, \forall i,} \\
& \cancel{\text{C9} : \mathbf{W_i} \succeq \mathbf{0}, \forall i,} \\
& \text{C10} : \tau_i \leq \ d_i \left(B_1 + B_2 - F_1 - F_2\right). \qquad (35)
\end{aligned}
$$

It is clear that C3' defines an oblique manifold [51] which can be noted by

$$\mathcal{O} = \{\mathbf{u} \in \mathbb{C}^N | [\mathbf{u}\mathbf{u}^H]_{n,n} = 1, \ \forall n \in N\}. \qquad (36)$$

And C3' is automatically satisfied when the optimal value of $\mathbf{u}$ is found over the while oblique manifold $\mathcal{O}$.

The Lagrange function [31] $\mathcal{L}(\mathbf{u}, \mu, \nu, \lambda)$, the Lagrange dual function [31] $D(\mu, \nu, \lambda)$ and the

Euclidean gradient of the Lagrangian function [31] $\mathrm{grad}_{\mathrm{u}} f$ must be introduced as a foreshadowing before explicitly applying the OMO technique.

At first, the Lagrange function $\mathcal{L}(\mathbf{u},\mu,\nu,\lambda)$ for P4 can be defined as

$$
\begin{aligned}
\mathcal{L}' =& \mathcal{L}(\mathbf{u},\mu,\nu,\lambda) \\
=& \sum_{i\in\mathcal{L}} \tau_i - \mu_n(\text{C3'}) - \nu_i(\text{C5'}) - \lambda_i(\text{C10}) \\
=& \sum_{i\in\mathcal{L}} \tau_i \\
& - \sum_{n} \mu_n \left(|u_n| - 1\right) \\
& - \sum_{i} \nu_i \left(\beta_i \mathrm{Tr}\left(\mathbf{W}_i \mathbf{P}_i^H \mathbf{u_n} \mathbf{u_n}^H \mathbf{P}_i\right) - d_i \gamma_{\min} \left(\sum_{k\in\mathcal{L}\setminus\{i\}} \beta_i \mathrm{Tr}\left(\mathbf{W}_k \mathbf{P}_i^H \mathbf{u_n} \mathbf{u_n}^H \mathbf{P}_i\right) - \beta_i \mathrm{Tr}\left(\mathbf{A} \mathbf{P}_i^H \mathbf{u_n} \mathbf{u_n}^H \mathbf{P}_i\right) \right) - \sigma_i^2 \right) \\
& - \sum_{i} \lambda_i \left(\tau_i - d_i \left(B_1 + B_2 - F_1 - F_2\right)\right), \qquad (37)
\end{aligned}
$$

where μ_n, ν_i, and λ_i are the Lagrange multipliers [31] associated with constraints C3', C5', and C10, respectively. Those Lagrange multipliers are unveiled to incorporate constraints C3', C5' and C10 into the optimization problem, which help to ensure these complex mathematical relationships are satisfied and maintained during the optimization process.

Secondly, the Lagrangian dual function $D(\mu,\nu,\lambda)$ is also introduced to be maximised to find the best values of Lagrange multipliers that satisfy the constraints leading to the maximum objective function. $D(\mu,\nu,\lambda)$ can be represented by

$$
D(\mu,\nu,\lambda) = \inf_{\mathbf{u}} \mathcal{L}(\mathbf{u},\mu,\nu,\lambda), \qquad (38)
$$

where inf indicates the infimum of the Lagrangian function $\mathcal{L}(\mathbf{u},\mu,\nu,\lambda)$ with respect to the variable $\mathbf{u}$.

Eventually, the gradient of the Lagrange function $\mathrm{grad}_{\mathrm{u}} f$ onto the tangent space is introduced to find the critical points for the Lagrangian dual function $D(\mu,\nu,\lambda)$ which can further lead to the optimal solutions in the end. Additionally, setting the gradient to zero is a traditional way to find the stationary points which also indicate critical points. The gradient of the Lagrange function can be expressed as

$$
\begin{aligned}
\mathrm{grad}_{\mathrm{u}} f &= \nabla_{\mathbf{u}} \mathcal{L}(\mathbf{u}, \mu, \nu, \lambda) \\
&= \begin{bmatrix} \frac{\partial \mathcal{L}}{\partial u_1} \\ \frac{\partial \mathcal{L}}{\partial u_2} \\ \vdots \\ \frac{\partial \mathcal{L}}{\partial u_n} \end{bmatrix} \\
&= \frac{\partial}{\partial \mathbf{u}} \sum_{i \in \mathcal{L}} \tau_i \\
&\quad - \frac{\partial}{\partial \mathbf{u}} \left(\sum_n \mu_n (|\mathbf{u}_n| - 1) \right) \\
&\quad + \frac{\partial}{\partial \mathbf{u}} (\sum_i \nu_i \left(\beta_i \mathrm{Tr} \left(\mathbf{W}_i \mathbf{P}_i^H \mathbf{u} \mathbf{u}^H \mathbf{P}_i \right) \right. \\
&\quad - \frac{\partial}{\partial \mathbf{u}} \left(\nu_i d_i \gamma_{\min} \sum_{k \in \mathcal{L} \setminus \{i\}} \beta_i \mathrm{Tr} \left(\mathbf{W}_k \mathbf{P}_i^H \mathbf{u} \mathbf{u}^H \mathbf{P}_i \right) \right) \\
&\quad + \frac{\partial}{\partial \mathbf{u}} \nu_i \left(-d_i \gamma_{\min} \beta_i \mathrm{Tr} \left(\mathbf{A} \mathbf{P}_i^H \mathbf{u} \mathbf{u}^H \mathbf{P}_i \right) - \sigma_i^2 \right) \\
&\quad - \frac{\partial}{\partial \mathbf{u}} \sum_i \lambda_i \left(\tau_i - d_i \left(B_1 + B_2 - F_1 - F_2 \right) \right), \\
&= 0 \\
&\quad - \sum_n \mu_n \frac{|\mathbf{u}_n|}{\mathbf{u}_n} \\
&\quad - \sum_i \nu_i \frac{\partial}{\partial \mathbf{u}} \left(\beta_i \mathrm{Tr} \left(\mathbf{W}_i \mathbf{P}_i^H \mathbf{u} \mathbf{u}^H \mathbf{P}_i \right) \right) \\
&\quad + \sum_i \nu_i d_i \gamma_{\min} \frac{\partial}{\partial \mathbf{u}} \left(\sum_{k \in \mathcal{L} \setminus \{i\}} \beta_i \mathrm{Tr} \left(\mathbf{W}_k \mathbf{P}_i^H \mathbf{u} \mathbf{u}^H \mathbf{P}_i \right) \right) \\
&\quad - \sum_i \nu_i d_i \gamma_{\min} \frac{\partial}{\partial \mathbf{u}} \left(\beta_i \mathrm{Tr} \left(\mathbf{A} \mathbf{P}_i^H \mathbf{u} \mathbf{u}^H \mathbf{P}_i \right) \right) - 0 \\
&\quad + \frac{\partial}{\partial \mathbf{u}} \sum_i \lambda_i \left(d_i \left(B_1 + B_2 - F_1 - F_2 \right) \right).
\end{aligned} \tag{39}
$$

In conclusion, P4 can be solved by an iterative optimization algorithm. The objective of this algorithm is to find the optimal solution for $\mathbf{u}$ that maximizes the utility function $\sum_{i \in \mathcal{L}} \tau_i$ while satisfying the constraints C3', C5', and C10. Numerical optimization methods are like gradient ascent, Newton's method, and constrained optimization solver.

Consequently, the OMO algorithm Algorithm 2 fully contains the above gradient-based techniques and starts with one stationary point of an oblique manifold. Every point in this

oblique manifold will be covered through the iteration and the optimal value of $\mathbf{u}^*$ can be found in the end.

Algorithm 2 Oblique Manifold Optimization (OMO) for Subproblem 4

1: **Initialize:** Set iteration index $n = 0$, choose an initial guess for $\mathbf{u}_0$, set convergence tolerance ε.
2: **Initialize:** $\{W_i^*\}, A^*$
3: **repeat**
4: Formulate the Lagrangian $\mathcal{L}(\mathbf{u}, \mu, \nu, \lambda)$ according to Problem P5.
5: Compute the gradient $\text{grad}_{\text{u}} f$.
6: Update $\mathbf{u}$ using a numerical optimization method to maximize $\sum_{i \in \mathcal{L}} \tau_i$.
7: Set $n = n + 1$
8: **until** Convergence criteria met: $\text{grad}_{\text{u}} f < \varepsilon$
9: **Output:** Optimal Set $\mathbf{u}^* = \mathbf{u}_n$.

At last, the alternating optimization algorithm Algorithm 3 is promoted to find the optimal solutions of the Problem Formulation (P0) through a combination of four iteration loops, Algorithm 1 and Algorithm 2. By setting the height of UAV z and the selecting parameter d_i as a stationary value separately and sequentially, Algorithm 1 and Algorithm 2 can proceed together with a proper manner.

Algorithm 3 Alternating Optimisation Algorithm

Initialize: Set iteration index $t = 1$, the initial point $\mathbf{u}^{(1)}$, binary index $k = 1$, select factor $d_{(k)}^{(t)}$, total number of LU $\mathcal{L}$, convergence tolerance ω.
Input: UAV's initial height $z^{(t)} = \mathcal{Z}_{\min}$, $d_{(k)}^{(t)} = 0$
repeat
    repeat
        repeat
            repeat
                Solve P3 via Algorithm 1 for given $\mathbf{u}^{(t)}$, $z^{(t)}$ and $d_{(k)}^{(t)}$ and store the optimal solution $W^{(t)}$ and $A^{(t)}$
                Solve P4 via Algorithm 2 for given $W^{(t)}$, $A^{(t)}$, $z^{(t)}$ and $d_{(k)}^{(t)}$ store the optimal solution $\mathbf{u}^{(t+1)}$
                Set $k = k+1$, $d_{(k)}^{(t)} = |d_{(k)}^{(t)} - 1|$
            until Convergence criteria met: $|f^{(t+1)} - f^{(t)}| \leq \omega$
        until $k > 2$
        Set $z^{(t)} = z^{(t)} + 1$, $k = 1$
    until $z^{(t)} > \mathcal{Z}_{\max}$
    Set $t = t+1$, $z^{(t)} = \mathcal{Z}_{\min}$
until $t > \mathcal{L}$
Output: Obtain the solution by $z^* = z$, $\mathbf{d}^* = \mathbf{d}$, $W_i^* = W_i^{(t)}$, $A^* = A^{(t)}$, and $\mathbf{u}^* = \mathbf{u}^{(t)}$

Chapter 6

Simulation Results

In this chapter, the simulation results of the designed algorithm for the established system model are demonstrated. Additionally, the simulations about the average minimum secrecy rate per user with different conditions are completed by MATLAB.

6.1 Simulation preparation

A three-dimensional coordinate system is established shown in Figure 6.1 to reflect the outlined system model shown in Figure 4.3 in section 4.1.

As introduced in the promoted system, the channels between the UAV-assisted IRS and the LUs as well as the UAV-assisted IRS and the EDs follow a frequency flat Rician fading channel model with an altitude-dependent Rician factor. The final goal is to plot the average minimum secrecy rate per user which is the primal evaluation standard for the performance of the designed algorithm. The fundamental parameters such as the numbers of LUs and EDs, the maximum number of SUs, the minimum and maximum height of UAV, the number of reflecting elements of IRS, the SINR value used to select the user to sacrifice, the maximum transmitting power of BS and Antenna number of BS. The BS is set to be located in the centre of the whole system region with a radius of 200m. Besides, some other parameters not mentioned in the system model but necessary for simulation progress such as the bandwidth, the antenna gains of the transmitting antenna and receiving antenna, the average channel power gain and the path loss coefficient are also listed. All the essential parameters are listed in Figure 6.2.

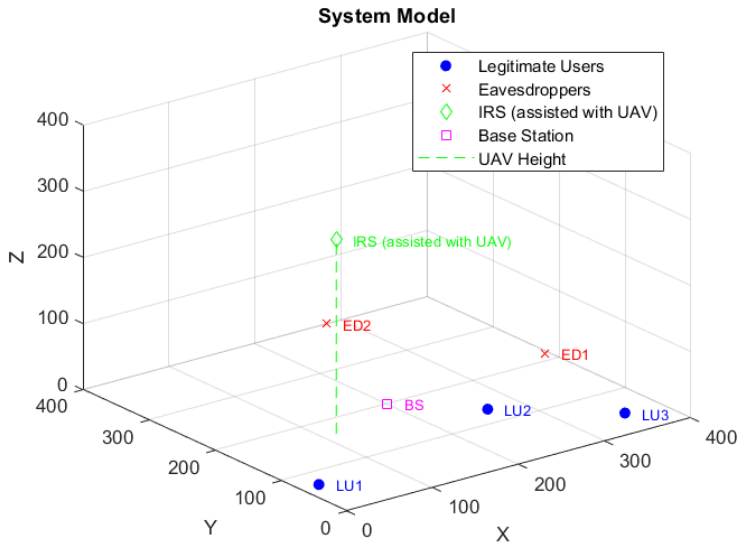

Figure 6.1: The system model in a 3-D coordinate

Parameter	**Physical meaning**	**Value**
$\mathcal{L}$	Number of LUs	3
$\mathcal{M}$	Number of EDs	2
$\mathcal{D}_{max}$	Maximum number of SUs	3
$\mathcal{Z}_{min}$	Minimum height of UAV	50m
$\mathcal{Z}_{max}$	Maximum height of UAV	400m
N	reflecting elements of IRS	30 ˜190
γ_{min}	Any LUs less than this SINR will be selected as SU	10 dB
P_{BS}	Maximum transmitting power of BS	46 dBm
$\mathrm{N_T}$	Antenna number of BS	3, 6, 9
B	Bandwidth	200 kHZ
f_c	Carrier frequency	2.0 GHz
G_t	TX antenna gain	0 dB
G_r	RX antenna gain	0 dB
β_0	Average channel power gain	-50 dBW
n	Path loss coefficient	2

Figure 6.2: Simulation Parameter

6.2 Secrecy rate simulation

It is distinct that several observations can be found in Figure 6.3. In the first place, the average minimum secrecy rate goes higher while the transmit power budget is amplifying. At the same time, adding more antennas can also benefit the security level of the whole system. However, it is significant that the gap between the $N_T = 3$ curve and the $N_T = 6$ curve is smaller than the gap between the $N_T = 6$ curve and the $N_T = 9$ curve. These safety-benefiting differences become less significant as the number of equipped antennas increases, which also reflects one trade-off between the secrecy rate and the consumption of the transmit power budget under the resource allocation background. The same principle of resource allocation also suits the relationship between the transmit power budget and the average minimum secrecy rate which has been discussed before, the slope of a single secrecy rate curve is decreasing and approaching a positive constant.

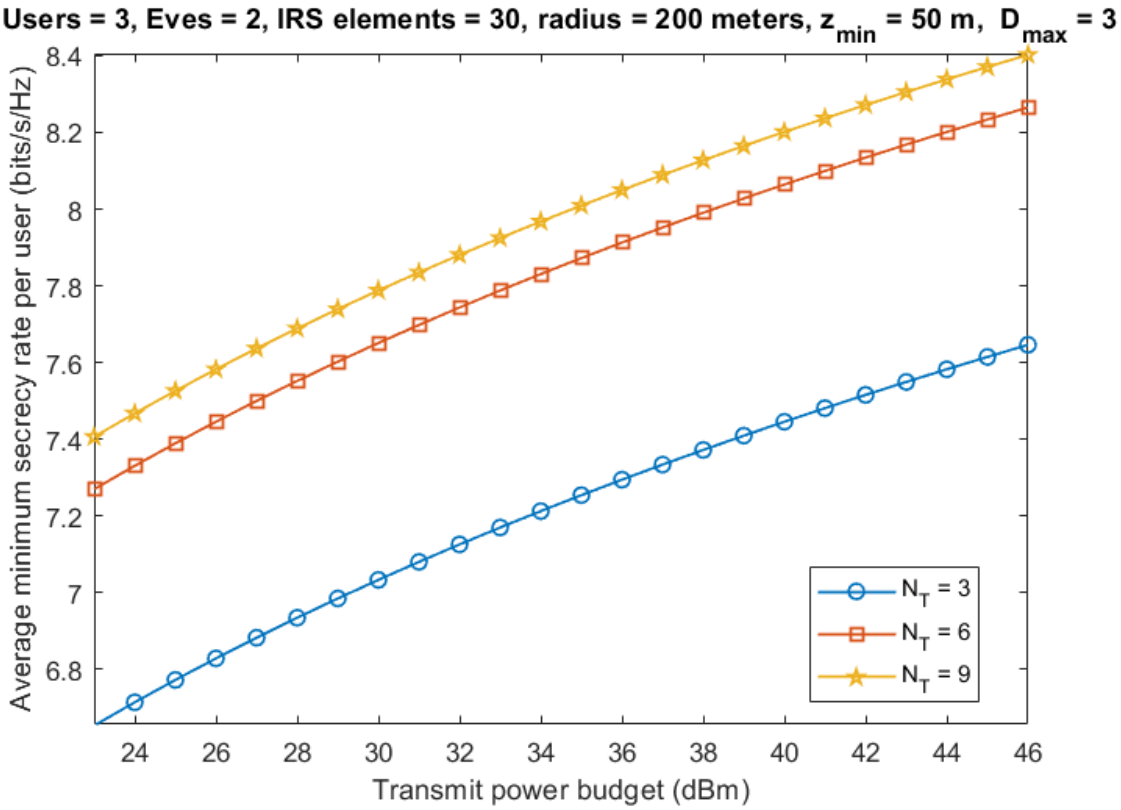

Figure 6.3: Average minimum secrecy rate per user with different Transmit power budget

Subsequently, compared with Figure 6.3, Figure 6.4 has two obvious similarities which are the trend of the secrecy rate curve and the tendency of positive slopes of those curves.

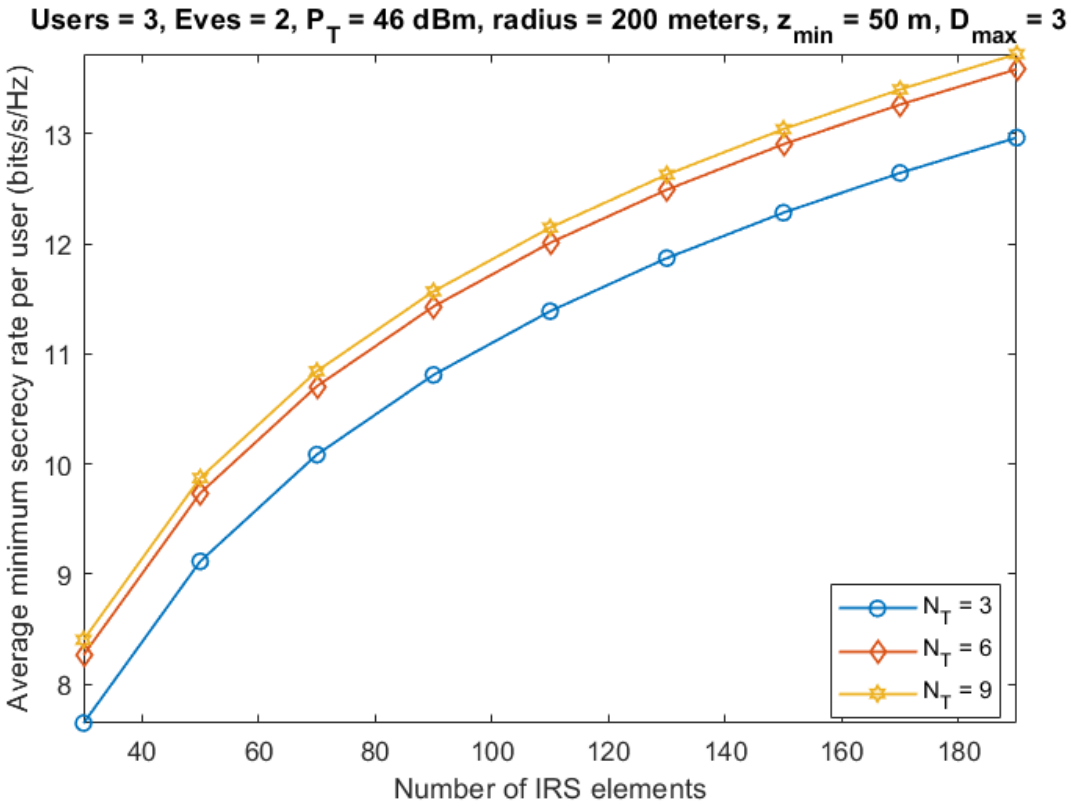

Figure 6.4: Average minimum secrecy rate per user with different Number of IRS elements

Nevertheless, all three average minimum secrecy rate curves vary dramatically even though there is a diminishing trend in the end, which indicates the slopes of the secrecy rate curves in the second graph are larger than in the first case.

As a result, both transmitting power and the number of IRS elements can influence the performance of the designed algorithm in the fabricated network and the number of antennas can also contribute to the improvement of the average minimum secrecy rate. The simulation results successfully prove the validity of the dedicated algorithm and also reveal the three main variables which are the number of antennas, the transmit power budget and the number of IRS elements that greatly affect the security of the wireless network system. The slope of different secrecy rate curves and the gap distance between different antennas in the same diagram are also bargaining chips for resource allocation which has different deliverables. The relationships between the average minimum secrecy rate per user and the number of antennas, the number of IRS elements, transmit power budget can be shown in Figure 6.5.

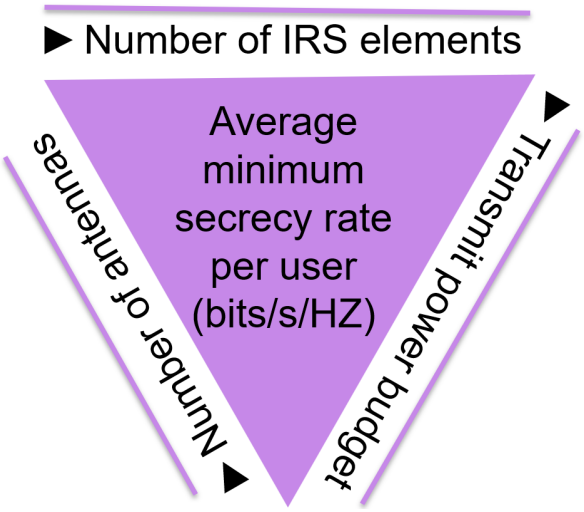

Figure 6.5: Several relationships reflected by the simulation

Chapter 7

Discussion

7.1 Conclusion

This thesis presents a detailed beamforming design for the IRS-assisted wireless network system, which aims at strengthening the PLS of the network. The system model is brought out to illustrate the various components within the network and the problem formulation is followed to describe the evaluating standard of the deliverable. A detailed algorithm design is promoted to tackle the announced problem formulation and its performance is displayed by the plots from the simulation progress. Through the analysis of the simulated secrecy rate of the whole system, additional trade-offs among the transmit power budget, the number of antennas, and the number of IRS elements in practical wireless communication scenarios within the context of resource allocation become evident.

7.2 Future work

The development of UAVs never remains stagnant due to its embedded system structure [53]–[58]. There are a number of aspects that can be upgraded potentially at the hardware level and software level. The factors with great development prospects at the hardware level such as the battery's life, the intelligence level of the embedded single-chip microcomputer, and the outer structure of UAV still have a lot of potential space to be improved. On the other hand, many advanced improvements can also be achieved at the software level, for example, the topology of the UAV network, the following the design of the advanced algorithm and the transmission data rates have occupied amounts of room for amelioration. Another potential evolution direction

of UAVs is how to increase the stability to deal with extreme environmental conditions and variations in the air. And this pathway also influences the coverage of the UAV. Besides, the size of the UAV also plays a very big role during its refinement and there always exists upper and lower limits on the size of drones that wait to be reached by the researchers.

Similar to the UAV, there is plenty of room for the IRS technology to develop as well. Firstly, the compatibility with the 6G network is a problem worthy of study. In the process of transmitting specific signals, the effective transmission efficiency of the IRS directly affects its compatibility. Secondly, the IRS can also be combined with Artificial Intelligence (AI) and Machine Learning (ML) [59], [60], [61], [62], [63], [64], [65]. [66], [67], [68], which have great potential as hot topics in contemporary times. Finally, the energy transmission efficiency of the IRS also has great room for development and improvement.

Bibliography

[1] L. F. Cranor and S. Greenstein, *The Future of Wireless Communications*, 2002, pp. 253–253.

[2] A. G. Mikerov, "From the history of electrical engineering IV: Maxwell's electromagnetic theory and its experimental confirmation," in *2015 IEEE NW Russia Young Researchers in Electrical and Electronic Engineering Conference (EIConRusNW)*, 2015, pp. 5–10.

[3] *IEEE PRESS SERIES ON ELECTROMAGNETIC WAVE THEORY*, 2022, pp. b1–b2.

[4] H. Holma, A. Toskala, and J. Reunanen, *Further Outlook for LTE Evolution and 5G*, 2015, pp. 423–432.

[5] S. Secgin, *Cellular Communication and 1G Systems*, 2023, pp. 51–56.

[6] H. G. Myung and D. J. Goodman, *Single Carrier FDMA*, 2008, pp. 37–59.

[7] J. L. Burbank, J. Andrusenko, J. S. Everett, and W. T. Kasch, *Second-Generation (2G) Cellular Communications*, 2013, pp. 250–365.

[8] K. Raith and J. Uddenfeldt, "Capacity of digital cellular TDMA systems," *IEEE Transactions on Vehicular Technology*, vol. 40, no. 2, pp. 323–332, 1991.

[9] L. L. Hanzo, L.-L. Yang, E.-L. Kuan, and K. Yen, *CDMA Overview*, 2004, pp. 35–80.

[10] J. Brown, B. Shipman, and R. Vetter, "SMS: The Short Message Service," *Computer*, vol. 40, no. 12, pp. 106–110, 2007.

[11] A. Kukushkin, *Third Generation Network (3G), UMTS*, 2018, pp. 121–172.

[12] H. Holma and A. Toskala, *Introduction to WCDMA*, 2010, pp. 47–59.

[13] A. Kukushkin, *High-Speed Packet Data Access (HSPA)*, 2018, pp. 173–204.

[14] *Introducing the 4G Mobile Adventure*, 2008, pp. 1–14.

[15] C. Cox, *Orthogonal Frequency Division Multiple Access*, 2014, pp. 67–85.

[16] X. Sun, D. W. K. Ng, Z. Ding, Y. Xu, and Z. Zhong, "Physical Layer Security in UAV Systems: Challenges and Opportunities," *IEEE Wireless Communications*, vol. 26, no. 5, pp. 40–47, 2019.

[17] Y. Sun, D. W. K. Ng, J. Zhu, and R. Schober, "Robust and Secure Resource Allocation for Full-Duplex MISO Multicarrier NOMA Systems," *IEEE Transactions on Communications*, vol. 66, no. 9, pp. 4119–4137, 2018.

[18] J. Zhang, J. Zhang, D. W. K. Ng, S. Jin, and B. Ai, "Improving Sum-Rate of Cell-Free Massive MIMO With Expanded Compute-and-Forward," *IEEE Transactions on Signal Processing*, vol. 70, pp. 202–215, 2022.

[19] *Emerging Technologies in Software, Hardware, and Management Aspects Toward the 5G Era: Trends and Challenges*, 2018, pp. 13–50.

[20] Y. Zhang, *Network Function Virtualization*, 2018, pp. 37–65.

[21] *Software Defined Networking Concepts*, 2015, pp. 21–44.

[22] H. Xie, J. Xu, Y.-F. Liu, L. Liu, and D. W. K. Ng, "User Grouping and Reflective Beamforming for IRS-Aided URLLC," *IEEE Wireless Communications Letters*, vol. 10, no. 11, pp. 2533–2537, 2021.

[23] A. Manikas, *Beamforming - Sensor Signal Processing for Defence Applications*, 2015.

[24] A. Yarali, *The Future of Wireless Communication with 6G*, 2023, pp. 53–63.

[25] X. Yu, V. Jamali, D. Xu, D. W. K. Ng, and R. Schober, "Smart and Reconfigurable Wireless Communications: From IRS Modeling to Algorithm Design," *IEEE Wireless Communications*, vol. 28, no. 6, pp. 118–125, 2021.

[26] L. You, J. Xiong, D. W. K. Ng, C. Yuen, W. Wang, and X. Gao, "Energy Efficiency and Spectral Efficiency Tradeoff in RIS-Aided Multiuser MIMO Uplink Transmission," *IEEE Transactions on Signal Processing*, vol. 69, pp. 1407–1421, 2021.

[27] Z. Wang, D. W. K. Ng, V. W. S. Wong, and R. Schober, "Robust Beamforming Design in C-RAN With Sigmoidal Utility and Capacity-Limited Backhaul," *IEEE Transactions on Wireless Communications*, vol. 16, no. 9, pp. 5583–5598, 2017.

[28] E. Shi, J. Zhang, D. W. K. Ng, and B. Ai, "Uplink Performance of RIS-Aided Cell-Free Massive MIMO System With Electromagnetic Interference," *IEEE Journal on Selected Areas in Communications*, vol. 41, no. 8, pp. 2431–2445, 2023.

[29] Q. Qi, X. Chen, D. W. K. Ng, C. Zhong, and Z. Zhang, "Robust Beamforming Design for SWIPT in Cellular Internet of Things," in *2019 IEEE/CIC International Conference on Communications in China (ICCC)*, 2019, pp. 523–528.

[30] D. Xu, V. Jamali, X. Yu, D. W. K. Ng, and R. Schober, "Optimal Resource Allocation Design for Large IRS-Assisted SWIPT Systems: A Scalable Optimization Framework," *IEEE Transactions on Communications*, vol. 70, no. 2, pp. 1423–1441, 2022.

[31] S. Boyd and L. Vandenberghe, *Convex Optimization*. Cambridge university press, 2004.

[32] T. H. Davenport and P. Michelman, *THE AI ADVANTAGE*, 2018, pp. 1–7.

[33] W. Cheng, X. Zhang, H. Zhang, and Q. Wang, "On-Demand based wireless resources trading for Green Communications," in *2011 IEEE Conference on Computer Communications Workshops (INFOCOM WKSHPS)*, 2011, pp. 283–288.

[34] J. Zhang, E. Björnson, M. Matthaiou, D. W. K. Ng, H. Yang, and D. J. Love, "Prospective Multiple Antenna Technologies for Beyond 5G," *IEEE Journal on Selected Areas in Communications*, vol. 38, no. 8, pp. 1637–1660, 2020.

[35] H. R. Everett and M. Toscano, *Unmanned Air Vehicles*, 2015, pp. 244–403.

[36] Y. Cai, Z. Wei, R. Li, D. W. Kwan Ng, and J. Yuan, "Energy-Efficient Resource Allocation for Secure UAV Communication Systems," in *2019 IEEE Wireless Communications and Networking Conference (WCNC)*, 2019, pp. 1–8.

[37] D. W. K. Ng and R. Schober, "Resource allocation for secure OFDMA decode-and-forward relay networks," in *2011 12th Canadian Workshop on Information Theory*, 2011, pp. 202–205.

[38] J. Liu, K. Xiong, Y. Lu, D. W. K. Ng, Z. Zhong, and Z. Han, "Energy Efficiency in Secure IRS-Aided SWIPT," *IEEE Wireless Communications Letters*, vol. 9, no. 11, pp. 1884–1888, 2020.

[39] V. Kumar, M. F. Flanagan, D. W. Kwan Ng, and L.-N. Tran, "On the Secrecy Rate under Statistical QoS Provisioning for RIS-assisted MISO Wiretap Channel," in *2021 IEEE Global Communications Conference (GLOBECOM)*, 2021, pp. 1–6.

[40] X. Chen, D. W. K. Ng, W. H. Gerstacker, and H.-H. Chen, "A Survey on Multiple-Antenna Techniques for Physical Layer Security," *IEEE Communications Surveys Tutorials*, vol. 19, no. 2, pp. 1027–1053, 2017.

[41] Z. Yin, W. Xu, R. Xie, S. Zhang, D. W. K. Ng, and X. You, "Deep CSI Compression for Massive MIMO: A Self-Information Model-Driven Neural Network," *IEEE Transactions on Wireless Communications*, vol. 21, no. 10, pp. 8872–8886, 2022.

[42] Z. T. Minson and H. M. Kwon, "Secrecy Rate of Relay and Intelligent Reflecting Surface Antenna-Assisted MIMO," in *MILCOM 2022 - 2022 IEEE Military Communications Conference (MILCOM)*, 2022, pp. 661–666.

[43] D. Xu, X. Yu, D. W. Kwan Ng, and R. Schober, "Resource Allocation for Active IRS-Assisted Multiuser Communication Systems," in *2021 55th Asilomar Conference on Signals, Systems, and Computers*, 2021, pp. 113–119.

[44] S. Hu, Z. Wei, Y. Cai, C. Liu, D. W. K. Ng, and J. Yuan, "Robust and Secure Sum-Rate Maximization for Multiuser MISO Downlink Systems With Self-Sustainable IRS," *IEEE Transactions on Communications*, vol. 69, no. 10, pp. 7032–7049, 2021.

[45] C. Wang, C.-C. Wang, Z. Li, D. W. K. Ng, K.-K. Wong, N. Al-Dhahir, and D. Niyato, "STAR-RIS-Enabled Secure Dual-Functional Radar-Communications: Joint Waveform and Reflective Beamforming Optimization," *IEEE Transactions on Information Forensics and Security*, vol. 18, pp. 4577–4592, 2023.

[46] M. Sinaie, D. Wing Kwan Ng, and E. A. Jorswieck, "Resource Allocation in NOMA Virtualized Wireless Networks Under Statistical Delay Constraints," *IEEE Wireless Communications Letters*, vol. 7, no. 6, pp. 954–957, 2018.

[47] Z. Wei, F. Liu, D. W. Kwan Ng, and R. Schober, "Safeguarding UAV Networks through Integrated Sensing, Jamming, and Communications," in *ICASSP 2022 - 2022 IEEE International Conference on Acoustics, Speech and Signal Processing (ICASSP)*, 2022, pp. 8737–8741.

[48] W. Huang, Q. Si, and M. Jin, "Alternating Optimization Based Low Complexity Hybrid Precoding in Millimeter Wave MIMO Systems," *IEEE Communications Letters*, vol. 24, no. 3, pp. 635–638, 2020.

[49] P. Di Lorenzo and S. Scardapane, "Distributed Stochastic Nonconvex Optimization and Learning based on Successive Convex Approximation," in *2019 53rd Asilomar Conference on Signals, Systems, and Computers*, 2019, pp. 1–5.

[50] Z. Ma, M. Zhao, Q. Chen, and P. Fan, "MIMO detection for high-order QAM constellations based on successive decision feedback semidefinite relaxation," in *Proceedings of the Fifth International Workshop on Signal Design and Its Applications in Communications*, 2011, pp. 173–176.

[51] P.-A. Absil, R. Mahoney, and R. Sepulchre, *Optimization Algorithms on Matrix Manifolds*. Princeton University Press, 2009.

[52] X. Shen, S. Diamond, Y. Gu, and S. Boyd, "Disciplined convex-concave programming," in *2016 IEEE 55th Conference on Decision and Control (CDC)*, 2016, pp. 1009–1014.

[53] Y. Sun, D. Xu, D. W. K. Ng, L. Dai, and R. Schober, "Optimal 3D-Trajectory Design and Resource Allocation for Solar-Powered UAV Communication Systems," *IEEE Transactions on Communications*, vol. 67, no. 6, pp. 4281–4298, 2019.

[54] Q. Wu, J. Xu, Y. Zeng, D. W. K. Ng, N. Al-Dhahir, R. Schober, and A. L. Swindlehurst, "A Comprehensive Overview on 5G-and-Beyond Networks With UAVs: From Communications to Sensing and Intelligence," *IEEE Journal on Selected Areas in Communications*, vol. 39, no. 10, pp. 2912–2945, 2021.

[55] X. Sun, D. W. K. Ng, Z. Ding, Y. Xu, and Z. Zhong, "Physical Layer Security in UAV Systems: Challenges and Opportunities," *IEEE Wireless Communications*, vol. 26, no. 5, pp. 40–47, 2019.

[56] Y. Cai, Z. Wei, R. Li, D. W. K. Ng, and J. Yuan, "Joint Trajectory and Resource Allocation Design for Energy-Efficient Secure UAV Communication Systems," *IEEE Transactions on Communications*, vol. 68, no. 7, pp. 4536–4553, 2020.

[57] Z. Wei, Y. Cai, Z. Sun, D. W. K. Ng, J. Yuan, M. Zhou, and L. Sun, "Sum-Rate Maximization for IRS-Assisted UAV OFDMA Communication Systems," *IEEE Transactions on Wireless Communications*, vol. 20, no. 4, pp. 2530–2550, 2021.

[58] Y. Zhou, F. Zhou, H. Zhou, D. W. K. Ng, and R. Q. Hu, "Robust Trajectory and Transmit Power Optimization for Secure UAV-Enabled Cognitive Radio Networks," *IEEE Transactions on Communications*, vol. 68, no. 7, pp. 4022–4034, 2020.

[59] J.-C. Chen, "Machine Learning-Inspired Algorithmic Framework for Intelligent Reflecting Surface-Assisted Wireless Systems," *IEEE Transactions on Vehicular Technology*, vol. 70, no. 10, pp. 10 671–10 685, 2021.

[60] C. Liu, X. Liu, D. W. K. Ng, and J. Yuan, "Deep Residual Learning for Channel Estimation in Intelligent Reflecting Surface-Assisted Multi-User Communications," *IEEE Transactions on Wireless Communications*, vol. 21, no. 2, pp. 898–912, 2022.

[61] K. Liu, F. Ke, X. Huang, R. Yu, F. Lin, Y. Wu, and D. W. K. Ng, "DeepBAN: A Temporal Convolution-Based Communication Framework for Dynamic WBANs," *IEEE Transactions on Communications*, vol. 69, no. 10, pp. 6675–6690, 2021.

[62] C. Liu, Z. Wei, D. W. K. Ng, J. Yuan, and Y.-C. Liang, "Deep Transfer Learning for Signal Detection in Ambient Backscatter Communications," *IEEE Transactions on Wireless Communications*, vol. 20, no. 3, pp. 1624–1638, 2021.

[63] W. Xu, Z. Yang, D. W. K. Ng, M. Levorato, Y. C. Eldar, and M. Debbah, "Edge Learning for B5G Networks With Distributed Signal Processing: Semantic Communication, Edge Computing, and Wireless Sensing," *IEEE Journal of Selected Topics in Signal Processing*, vol. 17, no. 1, pp. 9–39, 2023.

[64] W. Yuan, C. Liu, F. Liu, S. Li, and D. W. K. Ng, "Learning-Based Predictive Beamforming for UAV Communications With Jittering," *IEEE Wireless Communications Letters*, vol. 9, no. 11, pp. 1970–1974, 2020.

[65] Z. Wei, W. Yuan, S. Li, J. Yuan, and D. W. K. Ng, "Off-Grid Channel Estimation With Sparse Bayesian Learning for OTFS Systems," *IEEE Transactions on Wireless Communications*, vol. 21, no. 9, pp. 7407–7426, 2022.

[66] Y. Wang, Z. Gao, J. Zhang, X. Cao, D. Zheng, Y. Gao, D. W. K. Ng, and M. D. Renzo, "Trajectory Design for UAV-Based Internet of Things Data Collection: A Deep Reinforcement Learning Approach," *IEEE Internet of Things Journal*, vol. 9, no. 5, pp. 3899–3912, 2022.

[67] Y. Jin, J. Zhang, X. Zhang, H. Xiao, B. Ai, and D. W. K. Ng, "Channel Estimation for Semi-Passive Reconfigurable Intelligent Surfaces With Enhanced Deep Residual Networks," *IEEE Transactions on Vehicular Technology*, vol. 70, no. 10, pp. 11 083–11 088, 2021.

[68] C. Liu, W. Yuan, S. Li, X. Liu, H. Li, D. W. K. Ng, and Y. Li, "Learning-Based Predictive Beamforming for Integrated Sensing and Communication in Vehicular Networks," *IEEE Journal on Selected Areas in Communications*, vol. 40, no. 8, pp. 2317–2334, 2022.

Appendix 1

This session is reserved to prove *Theorem 1*.

First of all, it is noticeable that the proposed algorithm would stop consuming power to transmit information to the ith LU and allocate the saved energy to other LUs if $R_{d,i}$ is equal or less than 0, which results in the optimal beamforming vector for the ith becoming $\mathbf{w}_i^* = 0$ indicating that $\text{Rank}(\mathbf{W}_i) = 0$. Additionally, the same logic suits the case when $SINR_i < \gamma_{min}$.

Secondly, the optimal beamforming matrix $\mathbf{W}_i$ can be guaranteed to be $\text{Rank}(\mathbf{W}_i) = 1$ as long as $P_{\text{BS}} > 0$, $R_{d,i} > 0$ and $SINR_i \geq \gamma_{min}$. This can be verified by transforming equation 34 in another totally equal form

$$
\begin{aligned}
\underset{\mathbf{W}_i,\mathbf{A},\rho_i,\iota}{\text{maximize}} \quad & \sum_{i\in\mathcal{L}} \tau_i \\
\text{s.t..} \quad & \text{C1}', \text{C5}', \text{C7}, \text{C9}, \\
& \text{C10}'' : \tau_i \leq \; d_i \left(\overline{B_1} + \overline{B_2} - \widetilde{F_1} - \widetilde{F_2} \right), \\
& \text{C11} : \rho_i \leq \sum_{k\in\mathcal{L}} \beta_i \text{Tr}\left(\mathbf{W}_k \mathbf{P}_i^H \mathbf{u}\mathbf{u}^H \mathbf{P}_i\right) + \beta_i \text{Tr}\left(\mathbf{A}\mathbf{P}_i^H \mathbf{u}\mathbf{u}^H \mathbf{P}_i\right), \\
& \text{C12} : \iota \leq \sum_{k\in\mathcal{L}\setminus\{i\}} \beta_j \text{Tr}\left(\mathbf{W}_k \mathbf{G}_j^H \mathbf{u}\mathbf{u}^H \mathbf{G}_j\right) + \beta_j \text{Tr}\left(\mathbf{A}\mathbf{G}_j^H \mathbf{u}\mathbf{u}^H \mathbf{G}_j\right), \qquad (40)
\end{aligned}
$$

where $\overline{B_1} = \log_2\left(\rho_i + \sigma_i^2\right)$ and $\overline{B_2} = \log_2\left(\iota + \sigma_j^2\right)$, ρ_i and ι are auxiliary optimization variables.

Equation 40 is jointly convex and the Slater's condition holds at the same time. Furthermore, Slater's condition can result in strong duality which also indicates that the optimal solution can be found by solving this duality problem. As already discussed in Section 5.2.4, one popular method to tackle the duality problem is bringing in the Lagrangian function. Thus, the

Lagrangian function of Equation 40 corresponding to beamforming matrix $\mathbf{W}_i$ is presented by

$$\begin{aligned}\mathcal{L}'' = & \xi \sum_{i\in\mathcal{L}} \mathrm{Tr}\left(\mathbf{W}_i\right) - \sum_{i\in\mathcal{L}} \mathrm{Tr}\left(\mathbf{W}_i\mathbf{Y}_i\right) \\ & - \nu_i' \left(\beta_i \mathrm{Tr}\left(\mathbf{W}_i\mathbf{P}_i^H\mathbf{u}\mathbf{u}^H\mathbf{P}_i\right) - d_i\gamma_{\min} \sum_{k\in\mathcal{L}\setminus\{i\}} \beta_i \mathrm{Tr}\left(\mathbf{W}_k\mathbf{P}_i^H\mathbf{u}\mathbf{u}^H\mathbf{P}_i\right) - d_i\gamma_{\min}\beta_i \mathrm{Tr}\left(\mathbf{A}\mathbf{P}_i^H\mathbf{u}\mathbf{u}^H\mathbf{P}_i\right) - \sigma_i^2 \right) \\ & + \kappa \mathrm{Tr}\left(\left[\nabla_{\mathbf{W}} F_1\left(\mathbf{W}^i,\mathbf{Z}^i\right) + \nabla_{\mathbf{W}} F_2\left(\mathbf{W}^i,\mathbf{Z}^i\right)\right]^H \left(\mathbf{W}-\mathbf{W}^i\right)\right) \\ & - \psi_i \sum_{k\in\mathcal{L}} \beta_i \mathrm{Tr}\left(\mathbf{W}_k\mathbf{P}_i^H\mathbf{u}\mathbf{u}^H\mathbf{P}_i\right) + \Upsilon, \end{aligned} \tag{41}$$

where Υ stands for the collection of the optimization variables of the primal and dual problems and constant terms that are not relevant to the current proof. ξ, ν_i', κ and ψ_i are the scalar Lagrange multipliers associated with constraints C1, C5, C10" and C11. $\mathrm{Y}_i \in \mathbb{C}^{N_\mathrm{T}\times N_\mathrm{T}}$ is the Lagrange multiplier matrix associated with constraint C9. Subsequently, the dual problem of equation 34 is defined as

$$\underset{\substack{\mathbf{Y}_i\succeq\mathbf{0},\\ \xi,\nu_i',\kappa,\psi_i\geq 0}}{\text{maximise}} \; \underset{\substack{\mathbf{W}_i,\mathbf{A}\in\mathbb{H}^{N_\mathbf{T}},\\ \tau_i,\rho_i,\iota}}{\text{maximise}} \mathcal{L}\left(\mathbf{W}_i,\mathbf{A},\tau_i,\mathbf{Y}_i,\xi,\nu_i',\kappa,\psi_i\right). \tag{42}$$

The characteristic of optimal beamforming matrix $\mathbf{W}_i^*$ can be further explored by Karush-Kuhn-Tucker (KKT) conditions [31]. Specifically, the KKT conditions relevant to $\mathbf{W}_i^*$ are

$$\begin{aligned} & \mathrm{K1}: \xi^*,\nu_i'^*,\kappa^*,\psi_i^* \geq 0, \mathbf{Y}_i^* \succeq \mathbf{0}, \\ & \mathrm{K2}: \mathbf{Y}_i^*\mathbf{W}_i^* = \mathbf{0}, \\ & \mathrm{K3}: \nabla\mathbf{w}_i^*\mathcal{L}'' = \mathbf{0}, \end{aligned} \tag{43}$$

where $\xi^*,\nu_i'^*,\kappa^*,\psi_i^*$ and $\mathbf{Y}_i^*$ represent the optimal Lagrange multipliers for dual problem 42, and $\nabla\mathbf{w}_i^*\mathcal{L}''$ stands for the gradient vector of $\mathcal{L}''$. Additionally, K3 can be rewritten as

$$\mathrm{Y}_i^* = \xi^*\mathrm{I}_{N_\mathrm{T}} - \Delta, \tag{44}$$

where Δ is given by

$$\begin{aligned}\Delta = & \psi^*\mathbf{P}_i^H\mathbf{u}\mathbf{u}^H\mathbf{P}_i \\ & - \kappa^*\left(\nabla_{\mathbf{W}} F_1\left(\mathbf{W}^i,\mathbf{A}^i\right) + \nabla_{\mathbf{W}} F_2\left(\mathbf{W}^i,\mathbf{A}^i\right)\right). \end{aligned} \tag{45}$$

Defining the maximum eigenvalue of matrix Δ as $v_\Delta^{max} \in \mathbb{R}$. It is widely acknowledged that the probability of all the eigenvalues having the same value v_Δ^{max} is zero since the wireless channels are absolutely random. If $v_\Delta^{max} > \xi^*$, then Y_i^* is a negative semidefinite matrix which

totally violates K1. On the contrary, Y_i^* is a positive definite matrix with full rank if $v_\Delta^{max} < \xi^*$. In this situation, $\mathbf{W}_i^*$ should be a null matrix due to the equation in K2. However, $\mathbf{W}_i^* = \mathbf{0}$ is completely unrealistic since this is not an optimal solution for $P_{\max} > 0$ and $R_{d,i} > 0$. At the same time, there must be at least one optimal solution as $\xi^* > 0$ which complies with all the restrictions such as constraint C1'. Consequently, v_Δ^{max}=ξ^* is the necessary condition which guarantees the optimal solution and also results in Rank ($\mathbf{Y}_k$)=N_T -1.

Finally, a unit-norm vector $\mathbf{e}_\Delta^{max} \in \mathbb{C}^{N_\mathrm{T}}$ is created that has no common points with Y_i^* ($\mathbf{Y}_i^* \mathbf{e}_\Delta^{max} = \mathbf{0}$) to explore further about the optimal solution. Moreover, $\mathbf{e}_\Delta^{max}$ implies the eigenvector of matrix Δ in accordance with v_Δ^{max} with unit norm. As a result, the optimal beamforming matrix $\mathbf{W}_i^*$ is truly a rank-one with the form $\mathbf{W}^* = \zeta v_\Delta^{max} \left(v_\Delta^{max}\right)^H$ under the conditions $P_{\max} > 0$ and $R_{d,i} > 0$, where ζ is applied to alter $\mathbf{W}_i^*$ make sure that constraint C1 is always satisfied.